AD-A138 454 MEASURING THE TEMPERATURE COEFFICIENTS OF THE ELASTIC 1/2
CONSTANTS OF INDIUM PHOSPHIDE(U) AIR FORCE INST OF TECH
WRIGHT-PATTERSON AFB OH SCHOOL OF ENGI.. J K POE
UNCLASSIFIED DEC 83 AFIT/GE/EE/83D-59 F/G 9/1 NL

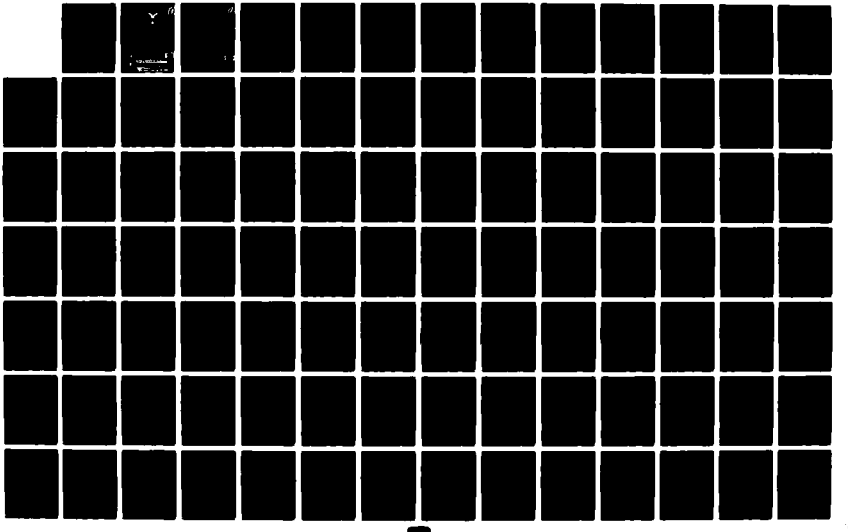

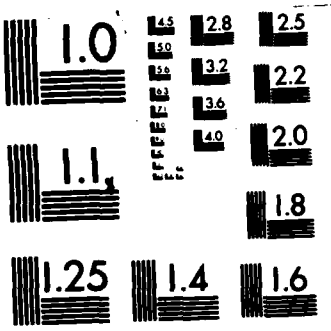

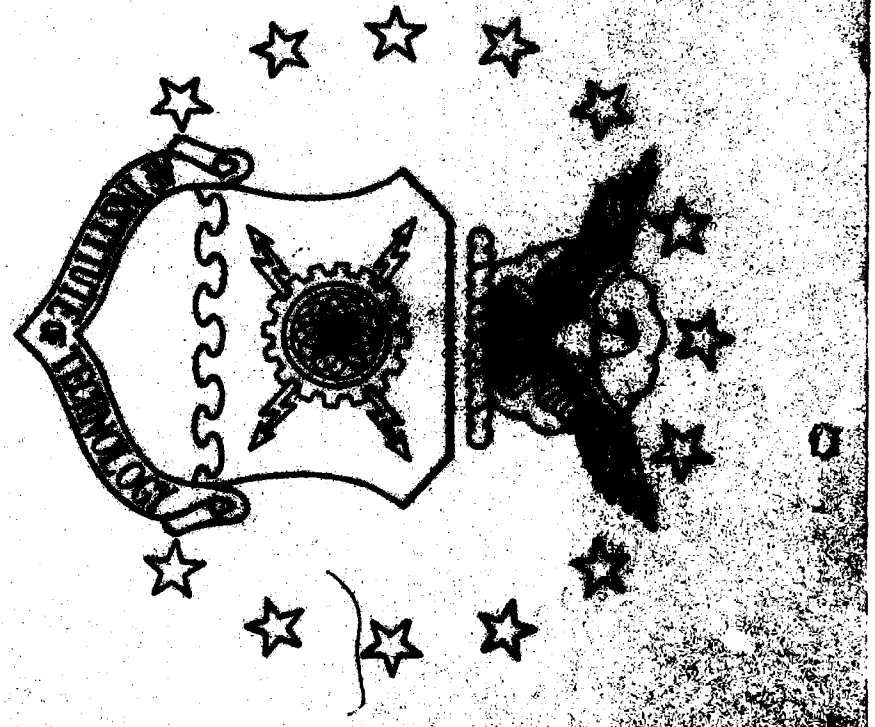

AFIT/GE/EE/83D-59

MEASURING THE TEMPERATURE COEFFICIENTS OF THE ELASTIC CONSTANTS OF INDIUM PHOSPHIDE

THESIS

Jonathan K. Poe, B.S.E.E.
2 Lt. USAF

AFIT/GE/EE/83D-59

AFIT/GE/EE/83D-59

MEASURING THE TEMPERATURE COEFFICIENTS OF THE ELASTIC CONSTANTS OF INDIUM PHOSPHIDE

THESIS

Presented to the Faculty of the School of Engineering

of the Air Force Institute of Technology

Air University

In Partial Fulfillment of the

Requirements for the Degree of

Master of Science in Electrical Engineering

by

Jonathan K. Poe, B.S.E.E.

2 Lt. USAF

Graduate Electrical Engineering

December 1983

Preface

The purpose of this research was to measure the elastic constants of Indium Phosphide (InP) over a range of temperatures. In conjunction with this work an experimental procedure and test set-up had to be designed and built. Previous investigations have indicated that InP has a strong potential for acoustic and electronic device applications.

This research is limited in scope to only measuring the elastic constants from 0.0°C to 45.0°C. I believe the theory, circuitry, and results to be complete and self-sufficient for the professional who undertakes the verification or continuation of this research. Anyone interested in purely measuring the elastic constants of an unknown through ultrasonic frequency methods should find this technique useful.

I would like to thank my advisor, Capt. Roger D. Colvin, Ph.D., of the Air Force Institute of Technology, Wright-Patterson AFB, Dayton, OH, and my sponsor, Mr. Andrew J. Slobodnik Jr. of the Rome Air Development Center, Hanscom Field, Bedford, MA for their timely guidance essential to the completion of this work. Deep gratitude is also expressed to my family at St. Mark's Episcopal, John and Ruby Webster, and Lynn Suzanne for providing me with much needed love and support.

Jonathan K. Poe

Table of Contents

	Page
Preface	ii
List of Figures	iv
List of Tables	vi
Abstract	vii
I. Introduction	I-1
Background	-1
Problem Statement	-3
Scope	-5
Approach and Presentation	-5
II. Resonator Theory and Methods of Measuring Elastic Constants	II-1
Background	-1
Resonator Theory	-1
Common Frequency Measurement Techniques	-5
Selection of an Appropriate Measurement Technique	-21
Development of a Technique for InP	-23
Desired Characteristics of InP Crystals	-25
III. Description of Test System and Data Collection	III-1
Theory of Test System	-1
Description of Test System	-2
Experimental Procedure	-11
Modified Measurement Technique for InP	-18
Theory for Modified Technique	-19
Modified Experimental Procedure	-25
Experimental Results	-27
IV. Conclusions and Recommendations	IV-1
Experimental System	-1
Summary of Data	-1
Material Characteristics	-12
Bibliography	BIB-1
Appendix A: Summary of Elastic Constant Characteristics	A-1
Appendix B: Test System Equipment List	B-1
Appendix C: InP Crystal Specifications	C-1
Appendix D: Experimental Data	D-1
Appendix E: Analysis of InP Characteristics	E-1

List of Figures

Figure		Page
II-1.	Graphic representation of tan $\gamma\alpha = \frac{\gamma\alpha}{k^2}$	II-2
II-2.	Typical measuring circuit for General Pulse Echo Technique	II-7
II-3.	Wave trains (echoes) and reflection phase shift for arrangement with transducer cemented directly to specimen	II-10
II-4.	Typical measuring circuit for the Phase Modulated Pulse Echo Technique	II-12
II-5.	Video patterns for the Phase Modulated Pulse Echo Technique	II-15
II-6.	Typical measuring circuit for "Sing-Around" High Frequency Technique	II-16
II-7.	Illustration of time difference between arrival of the trigger pulse and the triggering of the next pulse. Time difference is called trigger point delay	II-18
II-8.	Typical measuring circuit for the Continuous Wave Resonance Technique	II-20
III-1.	Typical response of signal strength versus frequency at resonance	III-1
III-2.	Schematic diagram of effect of FM deviation on resonant frequency	III-3
III-3.	Schematic block diagram of InP test system to measure resonant frequencies	III-5
III-4.	Schematic diagram of detailed circuitry for adjustment of input signal to oscilloscope	III-8
III-5.	Schematic diagram of power filter	III-8
III-6.	Schematic diagram for the control system of the analog integrator in the feedback loop	III-10
III-7.	Equivalent circuit for a section of transmission line with input and output terminals	III-19

Figure		Page
III-8.	Equivalent circuit for a piezoelectric transducer attached to InP single crystal	III-21
IV-1.	Frequency change vs. temperature for Thick Plate #11, <111> plane, shear wave propagation	IV-3
IV-2.	Frequency change vs. temperature for Thick Plate #22, <110> plane, shear wave propagation, type #1	IV-4
IV-3.	Frequency change vs. temperature for Thick Plate #22, <110> plane, shear wave propagation, type #2	IV-5
IV-4.	Frequency change vs. temperature for Thick Plate #22, <110> plane, longitudinal wave propagation	IV-6
IV-5.	Frequency change vs. temperature for Thick Plate #32, <100> plane, shear wave propagation	IV-7
IV-6.	C_{11} Elastic Constant vs. temperature	IV-8
IV-7.	C_{12} Elastic Constant vs. temperature	IV-9
IV-8.	C_{44} Elastic Constant vs. temperature	IV-10
A-1.	Plate orientations which yield pure modes of vibration	A-1
B-1.	Schematic block diagram of InP test system to measure resonant frequencies	B-2

List of Tables

Table		Page
II-1.	Summary of Characteristics for Pure Modes of Vibration for InP Research	II-5
III-1.	InP Elastic Constants at Room Temperature	III-31
III-2.	InP Wave Velocities at Room Temperature	III-32
A-1.	Elasto-Piezo-Dielectric Matrix for Cubic Crystals in Class 23	A-1
A-2.	Summary of Characteristics for Pure Modes of Vibration for Cubic Crystals of Class 23	A-2
D-1.	Thick Plate #11: <111> plane: shear wave propagation	D-1
D-2.	Thick Plate #22: <110> plane: shear wave propagation: type #1	D-2
D-3.	Thick Plate #22: <110> plane: shear wave propagation: type #2	D-3
D-4.	Thick Plate #22: <110> plane: longitudinal wave propagation	D-4
D-5.	Thick Plate #32: <111> plane: shear wave propagation	D-5
D-6.	Elastic Constants of InP	D-6
D-7.	Elastic Constants of InP	D-7
D-8.	Elastic Constants of InP	D-8
D-9.	C_{44} Elastic Constant of InP	D-9
D-10.	Elastic Constants of InP: Linear Regression Curve Fit Calculations	D-10
D-11.	Adjusted Elastic Constants of InP	D-11
E-1.	Analysis of InP Characteristics	E-1

Abstract

The temperature dependence of the elastic constants of Indium Phosphide (InP) was measured over the 0.0°C to 45.0°C temperature range. A modified Continuous Wave Resonance Technique was used to experimentally determine the values. The calculated temperature dependence was 60 ppm for the c_{11} elastic constant, 70.5 ppm for the c_{12} elastic constant, and 18 ppm for the c_{44} elastic constant. All are negative with increasing temperature. Such temperature behavior is consistent with similar studies of Indium Antimony (InSb), Gallium Phosphide (GaP), and Gallium Arsenide (GaAs).

The InP technique in this research applies the vibrational theory of small plates developed in 1963 by Tiersten in order to detect acoustic resonances in single crystal InP. The change in the resonant frequencies allows calculation of the acoustic wave velocity and corresponding effective elastic constant. By measuring the effective elastic constant for various plate orientations, the elastic constants of InP can be derived. Since InP is a cubic crystal of class 23 with a zinc-blende structure, measurements of the <111>, <110>, and <100> planes are sufficient to compute the elastic constants at a particular temperature. From such computations, changes in the elastic constants can be calculated with respect to temperature. Thus, temperature dependencies for the elastic constants of InP are derived.

The circuitry incorporating this InP technique utilizes a spectrum analyzer, an FM DC coupled signal generator, a high precision frequency

counter, and a Wayne-Kerr Bridge. In addition, an analog feedback loop was constructed to allow precision within 1 ppm. Such circuitry could easily be modified for automated data processing and higher precision. This technique and resulting circuitry could be applicable to measuring acoustic properties on any piezoelectrically excitable material as demonstrated by its success on X-cut quartz and InP in this research.

MEASURING THE TEMPERATURE COEFFICIENTS OF THE ELASTIC CONSTANTS OF INDIUM PHOSPHIDE

I. Introduction

Background

In the field of semiconductor devices, the major motivating factors to improve device technology are higher efficiency, output power, and speed, and lower cost, noise, and size. Indium Phosphide (InP) and other III-V semiconductor compounds exhibit considerably higher electron velocities than silicon (Si). [Ref. 2:7] This makes InP and other related III-V semiconductor compounds attractive for high speed device applications. In addition, InP has a higher peak-to-valley ratio, peak electron velocity, and thermal conductivity than Gallium Arsenide (GaAs). [Ref. 3:45] This makes InP extremely attractive for millimeter and microwave device applications.

InP research has grown since 1970 when Hilsum and Rees first proposed that semiconducting InP might offer advantages over GaAs in the area of Gunn device applications. [Ref. 6:277] Over the next decade with the Department of Defense (DoD) being the primary funder of most InP programs, InP research has gradually increased to include the areas of transferred electron devices (TED's), field effect transistors (FET's), electrooptics, and electronic devices. As with any device technology field, however, no matter how strong the arguments for improved device performance, nor how good the proven performance of the experimental or prototype version of the device, no device is viable until its material

technology is well developed and perfected. This is the case with InP. InP has shown great potential for electronic device applications. However, little is known about its physical parameters.

In another related field, the Rome Air Development Center (RADC) is currently investigating the temperature compensation of acoustic wave devices. As part of their investigation, RADC is searching for and testing various materials which have crystal orientations with low temperature coefficients of delay. Materials with this characteristic could then form acoustic devices that perform independent of temperature. In short, for these new materials and devices, the user need not be concerned with the temperature of operation.

InP is one such material with this potential of low temperature coefficients of delay. Thus there are two driving factors for InP research. Since InP is also a III-V semiconductor compound, the possibility exists for the fabrication of both acoustic and microwave frequency components on the same chip. If acoustic and electronic components can be fabricated on InP, semiconductor devices made of InP would have the advantages of smaller size, lighter weight, less noise, and lower power requirements. Acoustic devices would have low temperature dependence. Thus devices utilizing both semiconductor and acoustic properties would be possible.

Therefore, in order to fully exploit the potential advantages of InP, it is essential to develop accurate knowledge of the material characteristics of InP. For by knowing its material characteristics, InP can develop from a laboratory curiousity to a commercially available product.

Problem Statement

The first step toward making InP a commercially viable product is gaining knowledge of the crystal's electronic and acoustic properties. Among the basic parameters needed are the elastic constants. This research will therefore obtain the elastic constants of InP. The elastic constants of InP have only been measured at room temperature, and not over a range of temperatures. Thus the objective of this research is to measure the elastic constants of InP over a range of temperatures, 0.0°C to 45.0°C, along its three major independent axes. This would result in accurate knowledge of the elastic constants of InP and their temperature dependence. The next logical step after this completed research would be the manipulation of the data into matrix form. From here one could solve for the effective elastic constant and corresponding temperature coefficients in any direction. Since the major axes of InP are independent, directional dependence would just be a linear combination of the values of the three major axes.

These would be the first steps in obtaining knowledge about the elastic constants of InP. This completed research, however, will only accomplish the first step. This first step can be broken into several tasks.

The first task of this research is designing circuitry that takes into consideration the limitations inherent in the InP and is as simple and as accurate as possible. Simple means circuitry that is easy to use and understand. Circuitry that is easily procured and able to verify the results of this research fits into this definition of simplicity. Accurate means circuitry that measures just the elastic constants of InP

and not a quartz-glue-InP combination, nor the possible combined effective elastic, piezoelectric, and dielectric value of InP. Such circuitry will have to be flexible to measure over a range of temperatures. This task of designing such circuitry includes an extensive literature search to ensure that the requirements of simplicity, accuracy, and the limitations of the InP crystals are met.

The second task of this research in conjunction with the literature search is to verify that the circuitry works according to general acoustic and vibrational theory. Previous acoustic studies will be examined and analyzed for possible application to this research. Functional analysis will then be applied to insure that the resulting circuitry will work in accordance with the InP crystals.

The third task of this research is to build the designed circuitry and test it. The circuitry will be tested with X-cut quartz which is known to be acoustically resonant. Experimental data from the circuitry will be compared with the known results for X-cut quartz for verification.

The fourth task of this research is to perform the experiment on samples of InP single crystal and collect appropriate data. A major subtask of this area is to prepare the InP crystals for the experiment, if they are not already adequate. If the crystals must be sent to an outside agency or private contractor for preparation, a set of specifications and preparation instructions must be written. Another major subtask, if the primary InP measurement technique should prove to be unsuccessful, will be to design an alternate measurement technique. The alternate technique must try to incorporate as much of the original

primary technique as possible and yet succeed.

The fifth task of this research is to document the investigation and draw both conclusions and recommendations based on the results of the experiment. A major subtask of this area will be to make comments concerning any encountered difficulties and ways to prevent their occurrence. Suggestions for follow on studies will also be made.

Scope

This research will only measure the temperature coefficients of the elastic constants of InP. The temperature coefficients will only be presented for a temperature range from 0.0°C to 45.0°C. This range is more than adequate to determine the 1st and 2nd order temperature coefficients of the elastic constants of InP. Such information will provide a sufficient data base for InP devices that operate around room temperature. Furthermore, the temperature coefficients will only be measured along the major axes of the InP crystal, that is, the <100>, <110>, and <111> directions.

This research will not attempt to determine the temperature coefficients of the elastic constants of InP for any arbitrary direction or temperature. Such work is left to the interested reader or professional to complete.

Approach and Presentation

This research will mostly be presented in chronological order. Each chapter will discuss a different phase of the research and will also cover any problems encountered and their eventual resolution.

Chapter II will address the theory and problem analysis of acoustic

resonance. Section II-1 will cover the general background of the chapter. Section II-2 will discuss the general theory of vibration for arbitrarily oriented plates and how this theory relates to small crystals. Section II-3 will address the major acoustic techniques capable of measuring the elastic constants and discuss their various advantages and disadvantages. Section II-4 will center on completed acoustic research that measured the elastic constants of other materials applicable to this research on InP. It will also discuss how this research on InP developed from these previous methodologies. Section II-5 will address the constraints imposed by the InP crystals. Section II-6 will discuss the major characteristics of the InP crystals that were assumed in order that the elastic constants be derived.

Chapter III will address in detail the system selected to measure the elastic constants of InP, discuss those problems encountered in the collection of data, and finally, present the data. Section III-1 will address the theory behind the design of the system. Section III-2 will address the description of the system, both physical and functional aspects. Section III-3 will center on the procedure to measure the elastic constants of InP. It will also relate the procedure to the specified preparation requirements of the InP single crystals. It will also address the discrepancies between what was contracted for in terms of the crystal specifications and what was actually received. Section III-4 will discuss the modified experimental technique. Section III-5 will present the additional theory needed to understand the modified experimental technique. Section III-6 will center on the corresponding modified procedure to measure the elastic constants of InP. Section

III-7 will present the experimental results of the InP research and how they were derived.

Chapter IV will address the conclusions and recommendations based on the results of this research. Section IV-1 will address the experimental system. Section IV-2 will summarize the data collected. Section IV-3 will focus on the material characteristics of InP. Suggestions for follow on studies will also be made in this chapter.

II. Resonator Theory and Methods of Measuring Elastic Constants

Background

There exist many techniques for measuring the dynamic elastic constants of solids. The technique of measurement by ultrasonic frequencies can be divided into two broad categories. The first category involves the physical resonance of the specimen. In this case electromagnetic, electrostatic, or piezoelectric principles can be used to provide the necessary vibrations. The second category involves the propagation of travelling waves through the specimen. In this case the travelling waves can be continuous or pulse modulated. It is this latter category that has proved very useful in determining the elastic constants of small specimens, especially single crystals, as reported by Huntington. [Ref. 7:321] Therefore, this basic technique of wave propagation will be applied to determine the elastic constants of InP.

Resonator Theory

The foundation for all acoustic techniques employing travelling waves in small specimens is the theory of vibration. The general theory of vibration of arbitrarily oriented plates was studied extensively by Tiersten. [Ref. 15:35] [Ref. 19:53] His findings revealed that a mode of vibration involves three coupled elastic waves, and depends in a very complicated manner on all the elastic, piezoelectric, and dielectric constants of the material. In addition, the vibration also depends on the material density, thickness of the specimen, and the harmonic number of the frequency. Exact solutions, however, were developed only for

decoupled thickness modes in thin plates. [Ref. 19:55] According to Tiersten, they are:

$$\cos \gamma\alpha = 0 \qquad \text{(unstiffened)} \qquad (2\text{-}1)$$

$$\tan \gamma\alpha = \frac{\gamma\alpha}{k^2} \qquad \text{(stiffened)} \qquad (2\text{-}2)$$

where

$$\gamma\alpha = \frac{\omega T}{2}\left[\frac{\rho}{c_{eff}}\right]^{1/2} \qquad (2\text{-}3)$$

In these equations, ω is the resonant frequency, T is the thickness of the specimen, ρ is the material density, k is the piezoelectric coupling coefficient, and c_{eff} is the effective elastic constant. Since InP has piezoelectric coupling, this research is interested in the stiffened case. For better visual conceptualization, equation 2-2 is reproduced graphically below in Figure II-1. Note that the intersections of the tan $\gamma\alpha$ curve with the straight line of slope $1/k^2$ give the roots to the equation $\tan \gamma\alpha = \gamma\alpha/k^2$.

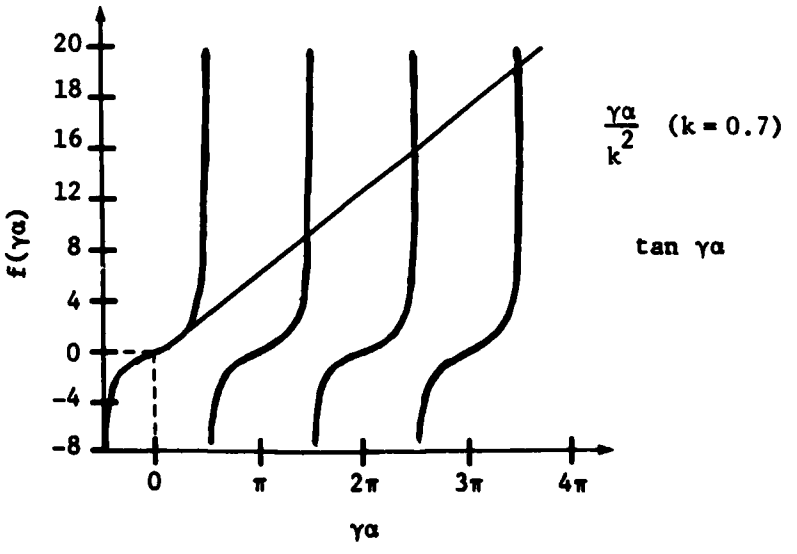

Figure II-1. Graphic representation of $\tan \gamma\alpha = \frac{\gamma\alpha}{k^2}$.

For high values of ω (high harmonic resonances), both equations 2-1 and 2-2 yield solutions of the form:

$$\frac{n\pi}{2} = \frac{\omega T}{2}\left[\frac{\rho}{c_{eff}}\right]^{1/2} \quad \text{(n odd)} \tag{2-4}$$

Thus the high harmonic resonant frequencies for the stiffened case and all resonant frequencies for the unstiffened case are given by:

$$f_{HH} = \frac{n}{2T}\left[\frac{c_{eff}}{\rho}\right]^{1/2} \tag{2-5}$$

The separation between successive high harmonic resonances is then:

$$\Delta f_{HH} = \frac{1}{T}\left[\frac{c_{eff}}{\rho}\right]^{1/2} \tag{2-6}$$

Since the density of InP is known to be 4.787×10^3 kg/m^3, [Ref. 4: 23] and T, the plate thickness, and Δf_{HH}, the separation between high harmonic resonances, are measureable quantities, equation 2-6 provides the means for determining the effective elastic constants as follows:

$$c_{eff} = \rho\,(T\,\Delta f_{HH})^2 \tag{2-7}$$

where two contacts are made on opposite sides of the crystal. As c_{eff} is related to the elastic, piezoelectric, and dielectric constants, measuring a sufficient number of Δf_{HH}'s allows calculation of enough c_{eff}'s in order to completely specify the coefficients of the elastic constant matrix of InP.

Since c_{eff} is a readily measureable quantity, all that remains is to relate this variable to the fundamental elastic constants of InP. This is accomplished by using the general theory of Tiersten (1963) and in

fact has been tabulated for other materials such as Bismuth Germanium Oxide (BGO), $Bi_{12}GeO_{20}$, by Onoe, Warner, and Ballman (1967). This summary of characteristics is reproduced below in Table II-1. Since InP is a cubic crystal of class 23, it has only three independent elastic constants. Therefore, relatively few measurements are needed for any given temperature, and attention can be focused to three plate orientations: <100>, <110>, and <111>. Thus knowing c_{eff} determines c_{11}, c_{12}, and c_{44}. It can be noted here that fields perpendicular to the major faces of a plate will always excite piezoelectrically stiffened modes, while unstiffened modes may or may not be excited by parallel fields. [Ref. 18:4]

Thus, by measuring c_{eff} as outlined above, and utilizing Table II-1, the entire elastic constant matrix of InP can be determined. In short, measuring Δf_{HH}, the separation between high harmonic frequencies, allows calculation of a unique c_{eff}, the effective elastic constant for a particular temperature and crystal orientation. Using the general theory of vibration as applied to small crystals, c_{eff} is broken down into a function of c_{11}, c_{12}, and c_{44}, the elastic constants of InP. By examining a sufficient number of different crystal orientations of InP over a range of temperatures, the temperature coefficients and the elastic constants can be determined. The task now remaining is to measure as precisely as possible Δf_{HH} for several specific cases of InP.

Common Frequency Measurement Techniques

Although there are numerous techniques for frequency measurements of acoustic resonances, the driving factors for this research were simplicity, accuracy, and the limitations of the InP crystals. There

TABLE II-1

Summary of Characteristics for Pure Modes of Vibration for InP

Plate Orientation	Mode	Excitation	Direction of Shear Displacement	Effective Elastic Constant c_{eff}	Electromechanical Coupling Factor k
<100>	Shear	$\parallel$	$\perp$ to field	c_{44}	---
<110>	Extensional	$\parallel$ to Z	---	$\frac{c_{11} + c_{12} + 2c_{44}}{2}$	---
	Shear	X	$\perp$ to normal and Z	$\frac{c_{11} - c_{12}}{2}$	---
	Shear	$\perp$	$\parallel$ to Z	$c_{44} + \frac{e_{14}^2}{\varepsilon_{11}}$	$\frac{e_{14}^2}{\varepsilon_{11} c_{eff}}$
<111>	Shear	$\parallel$	$\parallel$ to field	$\frac{c_{11} - c_{12} + c_{44}}{3}$	---

Note: For complete detailed characteristics, refer to Appendix A.

$\parallel$ - parallel.

$\perp$ - penpendicular.

X - not piezoelectrically excitable.

currently exist a number of continuous wave (CW) or pulse-echo techniques that accurately measure sound velocity. However, most of these systems are quite complex. [Ref. 17:792] Of the more simple systems to measure acoustic resonance, there are basically five major techniques.

General Pulse Echo Technique [Ref. 11:312]. This first technique is a high frequency method which was first proposed by Pellam and Galt in 1916. It was originally for liquids, but has also proved to be very useful for solids. In this technique a quartz transducer is cemented to one end of the specimen. A pulsed acoustic wave is then propagated through the crystal and allowed to resonate within the crystal. The reflected pulse is then detected so that the measurement of delay between successive pulse echoes can be made. Separate transducers for transmitting and receiving can also be used in this technique. For the generation of longitudinal waves X-cut quartz is recommended. For the generation of shear waves Y-cut quartz or AC-cut quartz is recommended. The operating frequency typically ranges from 5 to 1000 MHz. Figure II-2 shows a block diagram for a typical measuring circuit.

Although this technique is quite simple, great care must be taken in several areas. First, preparation of the major faces of the specimen must be precise. Flatness to $\pm$ 1500 angstroms, and parallelism to within 10 seconds of arc may be necessary, particularly for resonant frequencies above 100 MHz.

Second, the bond between the transducer and the specimen must be acoustically transparent. In selecting the type of glue, the question of whether longitudinal waves will be propagated, or shear waves, or both must be considered. Some glues or bonds are better than others depending

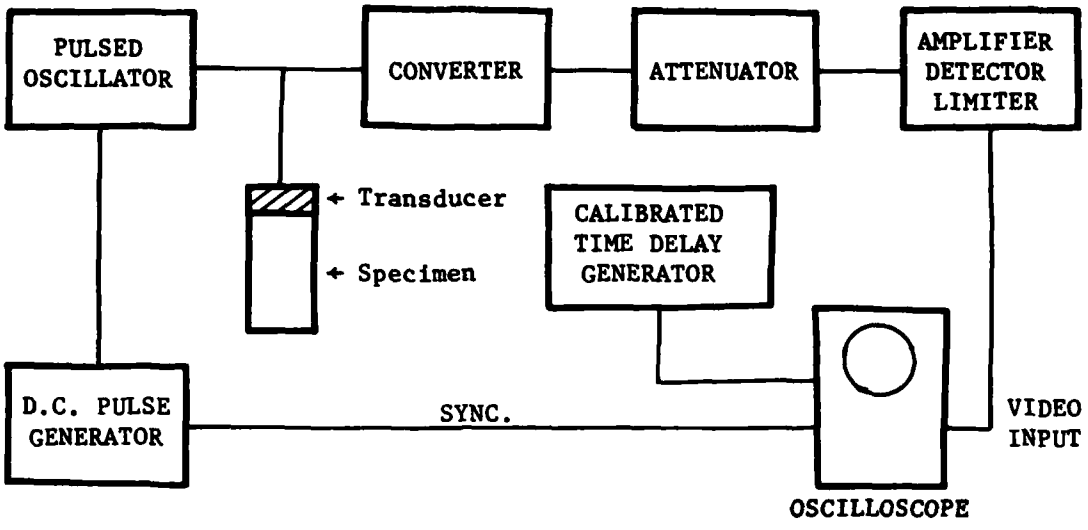

Figure II-2. Typical measuring circuit for General Pulse Echo Technique. [Ref. 11:313]

on the type of wave being propagated and the temperature variation. The novice researcher should refer to McSkimin (1967). [Ref. 12:25]

Third, acoustic losses in the bond need to be considered and accounted for. Such losses can be minimized by operating the crystal combination at the resonant frequency of the transducer. Depending on the type of glue used, a relatively high loss can occur at the frequencies just above resonance due to the stresses produced.

Fourth, other miscellaneous losses need to be considered. For instance, loss may occur due to the energy of the waves being absorbed electrically. This loss, however, is considerably less at resonance than it is slightly above resonance. The total reflection loss is another loss to be considered. Using symmetrical terminations and one

transducer for transmitting and receiving, a rough measurement of the total reflection loss can be obtained. Direct visualization of the instantaneous signal would provide a means of taking into account the transducer coupling effects. Yet direct visualization requires using a wide frequency bandwidth system. Also at high frequencies direct visualization may prove to be infeasible.

This technique has several advantages. First, coupling of the transducer is taken into account. This is important in accurately measuring the acoustic properties of just the specimen, and not a transducer-specimen compound. Second, direct visualization of the instantaneous amplitudes results in having velocity measurements accurate to within a few parts in 10^4. Third, the system can measure velocity as a function of varying environmental conditions such as temperature.

There are some disadvantages with this technique. First, a transducer must be bonded to the crystal. This results in having a less than pure measurement of the velocity due to only the specimen. Also coupling effects of the glue must be taken into account. Second, extensive crystal preparation is needed. Such preparation would add to the time and costs associated with this technique. Third, the crystal must be thick with respect to the transducer. This would eliminate the option of being able to measure small crystals. Fourth, the type of glue may severely limit the number of measurements feasible and the type of wave to be measured. This would restrict the size of the data base collected. Fifth, there are several miscellaneous losses associated with this technique.

Amplitude Modulated Pulse Echo Technique [Ref. 11:313] [Ref. 10:21].

This second technique is sometimes referred to as the Pulse Superposition Method. It utilizes the same physical arrangement of a crystal transducer cemented to the specimen as mentioned in the first technique with two significant differences. First, the transmitted waveform is more sophisticated to allow a higher confidence level of detection. Typical encoding schemes use a short duration RF pulse or train of waves (Figure II-3) constructed by a CW oscillator and a gate generator (Figure II-4). Second, if a pulsed acoustic wave is used, the pulse duration must be long enough to establish steady-state conditions with the transducer and glue. Therefore, τ, the time between any given crest in one echo and the corresponding crest in any other echo, will depend on several factors (Figure II-3). This relation is expressed in equation 2-8:

$$\tau = p\delta - \frac{p\gamma}{360f} + \frac{n}{f} \qquad (2\text{-}8)$$

where p is the number of round trips involved, δ is the round trip delay time which results from the specimen alone, γ is the phase angle measured in degrees at the frequency, f, and is associated with the reflection of acoustic waves at the transducer, f is the RF frequency in the pulse, and n is an integral number of periods. Since p is known and τ and f can be measured, n and γ must be determined in order to obtain a value for δ. Once δ is known, the velocity of propagation, v, can be determined using the relation:

$$v = \frac{2T}{\delta} \qquad (2\text{-}9)$$

where T is the thickness of the specimen.

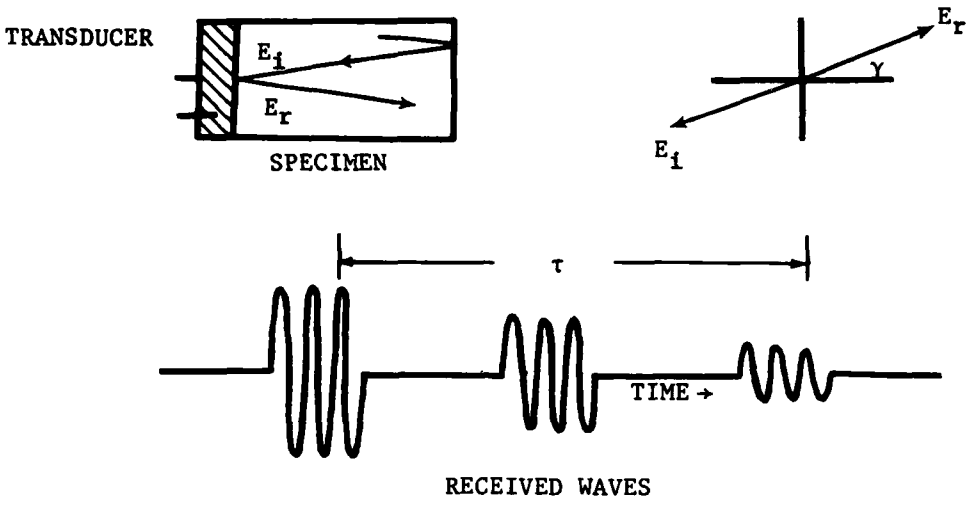

Figure II-3. Wave trains (echoes) and reflection phase shift for arrangement with transducer cemented directly to specimen. [Ref. 11:314]

If calculation of n proves difficult, equation 2-8 can be rearranged by noting that τ is a function of the wave frequency, f. For example, by making measurements at the resonant frequency of the transducer, f_o, and at f_L, a frequency 5 or 10% lower than f_o and applying equation 2-8 to each measurement, the subsequent relation is:

$$\Delta\tau = \frac{1}{f_L}\left(n - \frac{p\gamma_L}{360}\right) - \frac{1}{f_o}\left(n - \frac{p\gamma_o}{360}\right) \qquad (2\text{-}10)$$

where $\Delta\tau$ is the change between corresponding crests, γ_L is the phase angle at f_L, and γ_o is the phase angle at f_o. The right-hand side of equation 2-10 can then be evaluated for different thicknesses of the bond adhesive used. From such values a derivation of τ can be selected such that n = 0. Then the delay time, δ, is given by the relation:

$$\delta = \frac{\tau_o}{p} + \frac{\gamma_o}{360f} \qquad (2\text{-}11)$$

where τ_o is that value of τ when $n = 0$.

This technique has several advantages. First, coupling of the transducer is taken into account. Second, direct visualization of the instantaneous amplitudes are not necessary. Video pulses are used instead of the amplitude pulses. This eliminates the need for circuitry with extremely large frequency bandwidths. Third, the superposition of pulses provides good accuracy with δ easily determined to a few parts in 10^4. Fourth, this technique can measure velocity as a function of varying environmental conditions such as temperature.

There are some disadvantages with this method. First, the pulse duration must be long enough to establish steady-state conditions. High frequency measurements could prove to be difficult. Second, diffraction error could lead to lowered accuracy. Diffraction error is the error due to the travelling wave deviating from the original direction of propagation. Third, the specimen must be thick with respect to the transducer and carefully prepared. Crystal preparations must be similar to those discussed in the General Pulse Echo Technique. Fourth, a transducer must be bonded to the specimen. This results in having a less than pure measurement of the velocity due to only the specimen. Fifth, careful consideration must be used on the type and thickness of the glue. If τ, the change between crests, must be determined experimentally so that $n = 0$, several transducer-glue-specimen samples must be prepared. Sixth, as with General Pulse Echo Technique, there exist several miscellaneous losses associated with this technique which could lead to errors in

accuracy.

Phase Modulated Pulse Echo Technique [Ref. 11:315]. This third technique is sometimes referred to as the Phase Comparison Method since it obtains high accuracy through phase comparison. When combined with pulse techniques, this basic inherent accuracy of phase comparison can be used to good advantage in measuring wave velocities. This combination retains the advantage of being able to check alignments by direct visualization of the individual echoes. In addition, this combination easily determines velocities from frequency measurements. Figure II-4 illustrates a typical phase comparison pulse echo technique.

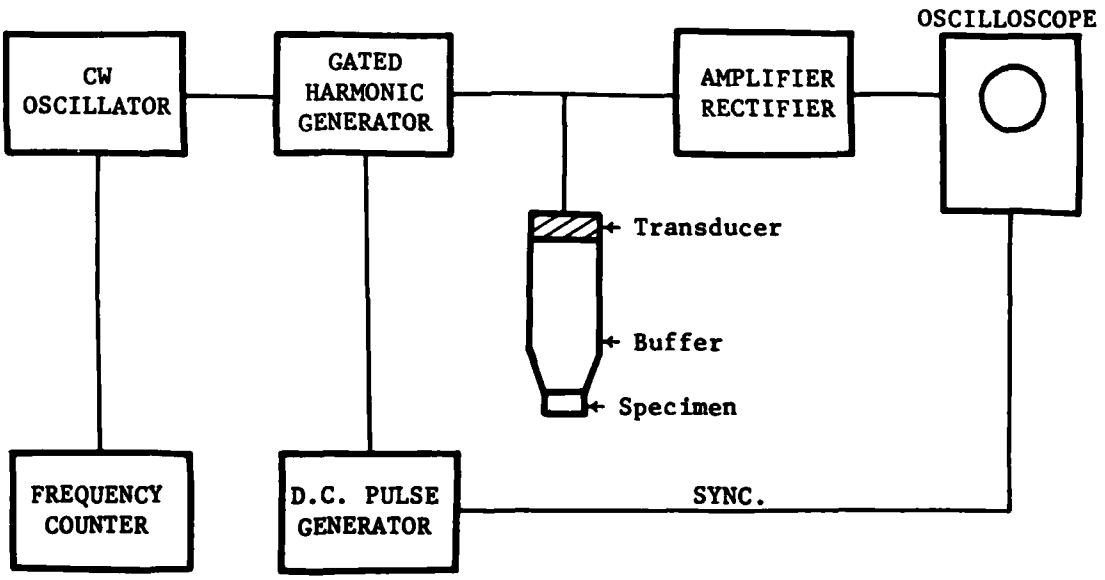

Figure II-4. Typical measuring circuit for the Phase Modulated Pulse Echo Technique.
[Ref. 11:315]

In such a system the pulsed waves produce a series of echoes by reflecting back and forth within the specimen. Temporarily disregarding

the effects of the transducer, the output voltage signals produced by any two successive echoes are as follows:

$$E_2 = E_1 A_r e^{j\gamma} \quad x \quad e^{-2\omega T/v} \tag{2-12}$$

where E_1 is the first received signal, E_2 is the second received signal, γ is the phase angle, ω is the frequency in radians, T is the thickness of the specimen, v is the velocity of propagation, and $A_r e^{j\gamma}$ is the product of the complex reflection coefficients for the reflections of waves at the end faces of the specimen.

If the echoes are exactly in phase, the phase components of E_1 and E_2 can be equated. The expression for the phase angles then becomes:

$$e^{-2\pi n} = e^{j\gamma} \quad x \quad e^{-2\omega T/v} \tag{2-13}$$

Taking the logarithm of both sides, equation 2-13 becomes:

$$-2\pi n = j\gamma - \frac{2\omega_n T}{v} \tag{2-14}$$

where ω_n is the frequency of the nth reflection in radians and n is an integer. From equation 2-14, solving for v gives:

$$v = \frac{2Tf}{n + (\gamma / 2\pi)} \tag{2-15}$$

where f_n is $\omega_n / 2\pi$.

For accurate results, n must be known without ambiguity even for approximate measurements, and likewise for γ, even though γ can sometimes be negligible. Accuracy results by McSkimin (1957) have been within a few parts in 10^4. [Ref. 12:25] Examining this phase comparison pulse echo technique in detail, gated harmonic generators or amplifiers can be

used instead of pulsed oscillators in order to provide more stable RF pulses. A suitable buffer rod can be made of an optical grade of strain-free fused silica. The specimen is attached to the end face of the rod opposite that attached to the transducer. Although some of the signal energy passes through the bond to produce echoes, in general, most of the energy is reflected at the interface. As previously mentioned, measurement of the relative amplitudes of the reflected wave and its first echo determines the phase angle, γ. By increasing the pulse duration, interference between echoes occurs. A distinctive video pattern occurs at f_n indicating that the waves are in-phase. This is illustrated in Figure II-5.

By obtaining the values of f_n over a wide range of frequencies, the integer, n, can be determined by the relation:

$$n \cong \frac{f_n}{\Delta f} \qquad (2\text{-}16)$$

where Δf is the frequency separation between adjacent values of f_n.

This technique has several advantages. First, evaluation of the transducer coupling effects can be made. This results in having velocity measurements accurate to within one part in 10^5. Second, very small specimens can be measured, such as crystals with linear dimensions as small as 2 millimeters. Third, the use of high frequencies minimizes errors due to diffraction and transducer coupling. Fourth, electrically conducting electrodes are not required on the specimen. Fifth, use of the buffer rod makes possible an optimized large passband transducer which will produce high quality pulses.

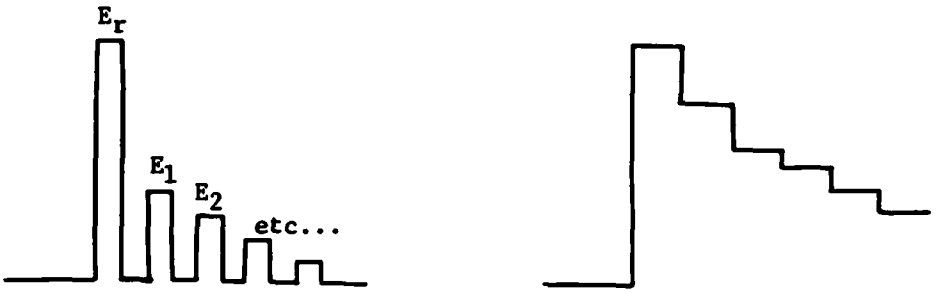

Figure II-5. Video patterns for the Phase Modulated Pulse Echo Technique. [Ref. 11:313]

In Figure II-5, E_r is the energy reflected at the buffer interface. E_1 and E_2, as previously mentioned, are the energies of successive pulses.

There are some disadvantages with this method. First, extensive preparation of the buffer rod may be necessary. Since the amplitude of the specimen-buffer rod interface reflection may be large with respect to the specimen pulses, bevelling the rod nearest the specimen may be necessary in order to reduce the incident energy on the rod-specimen interface. This would reduce the ratio of E_r to E_1, as shown in Figure II-5, and increase the chances of detecting E_1, E_2, etc... Second, thermal stress may occur as a result of the different thermal expansion coefficients. This would cause fracturing of the specimen and rod. Third, the seal problem for shear waves may drastically attenuate any return signal, especially at high temperatures. Fourth, this technique is not a good method for varying temperatures, although it is good for absolute temperature measurements.

Sing-Around High Frequency Technique [Ref. 2:963]. This fourth technique can be applied to both solids and liquids. In this method

separate transducers are used for transmitting and receiving the signal as illustrated in Figure II-6. A pulse is propagated through the specimen, detected, and used to trigger another pulse. This repetition rate of the series of pulses, sometimes called the pulse repetition rate (prf), can be accurately measured and thus determine the delay time, τ, and the velocity of propagation, v. Precision, however, is absolutely necessary in the measurement of the number of pulses in a known time interval and in the known length of the sonic course.

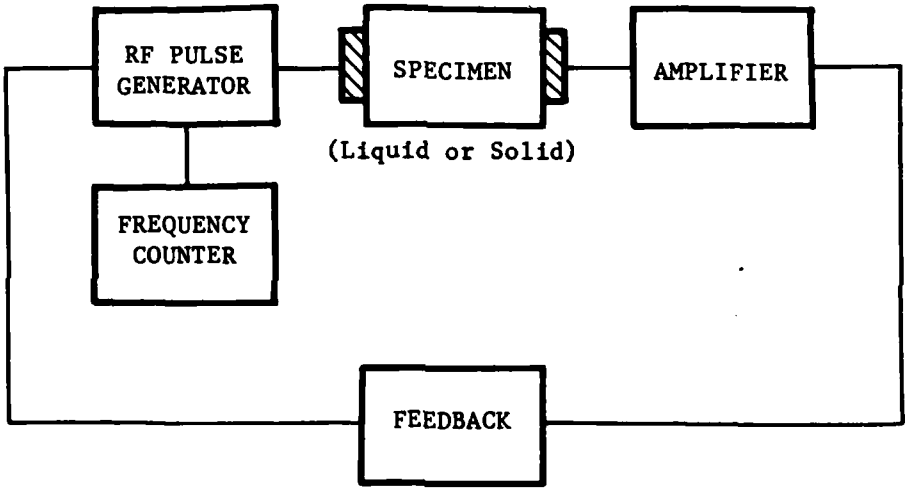

Figure II-6. Typical measuring circuit for "Sing-Around" High Frequency Technique. [Ref. 11:290]

The term sonic course is used because, unfortunately, the average time delay is made up of two components. The first is the desired acoustic delay due to the specimen. The second is the delay caused by the electronic circuits, the crystal transducer, and the crystal binder.

Since the electronic delay cannot be ignored, some means must be found to eliminate it from the calculations of the delay time. As a result, the delay time will strictly be a function of the specimen, and

not the electronic circuitry. The simplest way to eliminate the electronic delay is to use two specimens of different length under the same experimental conditions. The difference between the two average time delays represents the acoustic delay due to an acoustic path length equal to the difference between the two specimen lengths. This assumes that the electronic delays are the same for both specimens. This assumption, however, is not strictly justified and measures must be taken in order to minimize the differences in the electronic delay.

The electronic delay in turn is comprised of two components. The first component is the trigger point delay. The second component is the circuit delay resulting from the electronic circuitry. The trigger point delay exists because the successive pulses are not generated at the instant that the beginning of the trigger pulse arrives at the trigger point. The next pulse is initiated sometime later depending on the shape of the leading edge of the trigger pulse and the threshold voltage at which triggering is initiated. This is illustrated in Figure II-7.

Since each specimen measurement could have different trigger point delays, the difference in the two trigger point delays is the principal error in the acoustic delay time. In order to minimize this difference, the supply voltages must be stabilized, and the trigger pulses for the two specimens viewed on an oscilloscope. This allows one of the trigger pulses to be adjusted by means of the equipment gain controls so that the slope and amplitude of the leading edges of both trigger pulses are as nearly alike as possible.

The circuit delay which is caused by the rest of the electronic

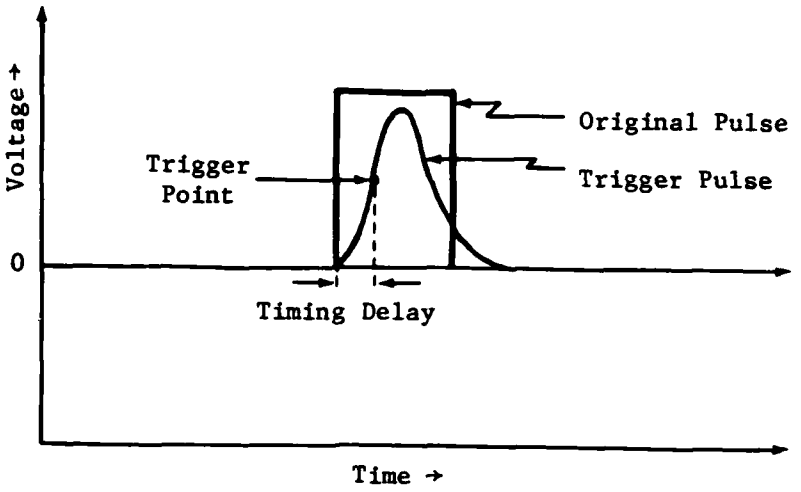

Figure II-7. Illustration of time difference between arrival of the trigger pulse and the triggering of the next pulse. The time difference is called trigger point delay. [Ref. 2:964]

circuits in the path traversed by the pulses mainly results in a second-order error. The difference in this delay time between the two specimens can be minimized. The differences in the delay times between the two specimens can be made negligible by using matched crystals and by ensuring that the total binder thickness is the same for both experiments.

There are several advantages to this technique. First, this method is particularly simple since RF modulation of the electrical pulse is eliminated, special pulse counting circuits are not employed, and a relatively simple detector-amplifier is sufficient for operation. Second, coupling effects of the transducer and electronic circuitry are taken into account by varying the specimen length. Third, precise measurements of specimen length result in absolute measurements accurate

to within a few parts in 10^8, and relative velocity changes to one part in 10^9. Fourth, the system can measure velocity as a function of varying environmental conditions such as temperature.

There are disadvantages with this method. First is the problem of errors due to the delay contributions of the system and transducer as well as in the accuracy of measuring the length of the specimens. Second, the effects of the amplitudes of the different pulses, not only between specimens, but also within individual experiments, can cause a loss in accuracy. Third, for each type of velocity measurement needed, two specimens must be prepared. Fourth, careful consideration must be used on the type and thickness of the glue. Nonuniformity could cause a significant difference in the delay times. Fifth, there are several miscellaneous losses associated with this technique such as reflection loss, diffraction loss, and circuit attenuation.

Continuous Wave Resonance Technique [Ref. 11:309]. This fifth technique was developed by Bolef and Menes in 1960 for high frequency resonance in the MHz range. The equipment used by this technique was minimal and very simple. The necessary equipment consisted of a standard Q-meter and a frequency measuring device, such as a counter, as illustrated in Figure II-8. In this technique a continuous acoustic wave is propagated through the crystal and monitored as its frequency is varied. A sudden drop in Q determines where the resonant frequency occurs. This drop can be determined with good accuracy. Only one transducer needs to be cemented to the specimen and very small specimens can be used if the frequency is very high.

This technique has several advantages. First, this method is par-

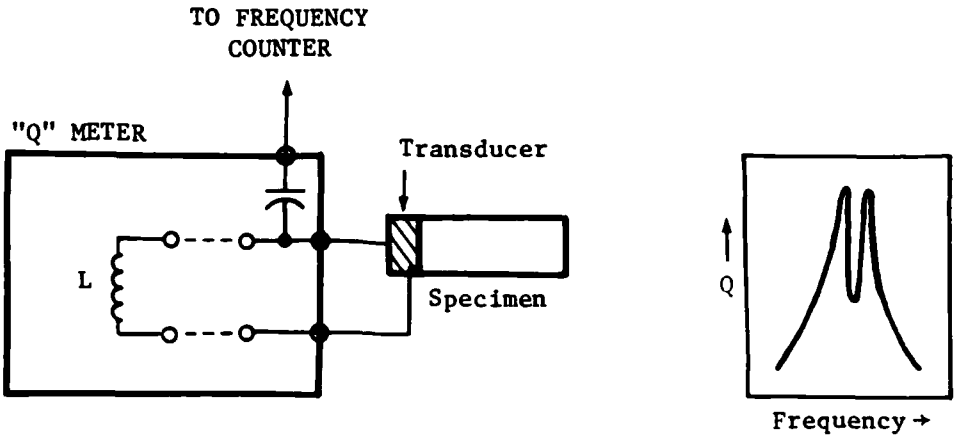

Figure II-8. Typical measuring circuit for the Continuous Wave Technique. [Ref. 11:309]

ticularly simple. Like the "Sing-Around" Technique, special pulse counting circuits are not employed, a relatively simple Q-meter is sufficient for operation, and RF modulation is not necessary. Second, measuring a relative drop in Q results in frequency measurements accurate to a few parts in 10^6. Third, use of high frequencies minimizes errors due to diffraction and transducer coupling. Fourth, very small specimens, as small as 1 millimeter, can be measured. Fifth, this method can measure velocity as a function of varying environmental conditions such as temperature or pressure.

There are disadvantages with this method. First, a transducer must be bonded to the specimen. This results in having a less than pure measurement of velocity due only to the specimen. Also coupling effects

of the glue must be taken into account. Second, extensive crystal preparations are needed. Crystal preparation must be similar to those discussed in the General Pulse Echo Technique. Third, there are some miscellaneous losses associated with this technique.

Selection of an Appropriate Measurement Technique

Any one of these five acoustic wave techniques could measure Δf_{HH}, the separation between high harmonic frequencies, or its inverse, $\Delta \tau_{HH}$, and thus calculate the elastic constants of InP. However, since the elastic constants are a very fundamental physical parameter for device technology, the accuracy of the measurements needs to be precise. In addition, the selected technique must also consider the limitations of the InP crystals. Third, the selected technique must also provide continuous readings as temperature is varied, and not require any recalibrations or other adjustments between readings. The technique that best satisfies these demands is the Continuous Wave Resonance Technique.

The most dominant factor affecting the choice of technique was the limitations of the crystals. The InP crystals were cut from two boules manufactured by RADC/ES, Hanscom Field, MA. The boules were grown by the Liquid Encapsulated Czochralski Method (LEC) from seed crystals that were directly synthesized from the elements Indium and Phosphorus. Direct synthesis was used to insure the highest starting level of purity possible. However, even though LEC growth has produced the largest InP single crystals [Ref. 8:iii], one of the boules twinned. Since it was desired to have as pure InP as possible, with a minimum number of impurities and dislocation densities, this result was expected. Thus the first limitation of the InP single crystals was size. Since the number

of impurities, dislocation densities, and the probability of twinning are all inversely related to each other, the demand for pure InP severely limited the size of the InP single crystals. The selected technique therefore had to measure acoustic resonances on small crystals.

The General Pulse Echo Technique and the Amplitude Modulated Pulse Echo Technique had the major disadvantages of not being able to measure small crystals, requiring a long time interval for steady-state conditions, and needing a transducer to be bonded onto the crystal. Although these disadvantages could be minimized, it would increase the complexity of the technique. They were therefore eliminated as preferred methods.

The Sing-Around Technique had the major disadvantages of the existence of trigger point delays, and the requirement of needing two nearly identical specimens per measurement. These could not be resolved without increasing the complexity of the technique. It was therefore eliminated as a preferred method. Thus the two best techniques for acoustic measurements in small crystals were the Phase Modulated Pulse Echo Technique and the Continuous Wave Resonance Technique. Yet in terms of simplicity, the Phase Modulated Pulse Echo Technique required the manufacturing of a buffer rod, whereas the Continuous Wave Resonance Technique did not. Furthermore, due to improvements as mentioned below, the Continuous Wave Resonance Technique was potentially more accurate than the other techniques. Thus the Continuous Wave Resonance Technique was selected as the preferred method for best overall satisfaction of the requirements of accuracy, simplicity, and the limitations of the InP crystals.

Development of a Technique for InP

Two previous studies have improved the Continuous Wave Resonance Technique applicable to this research on measuring the elastic constants of InP. The first study was done by Slobodnik and Sethares in 1971, and the second study was done by Melcher, Schickfus, and Baumann in 1981. In 1971 Slobodnik and Sethares refined an experimental technique originally developed by Onoe, Warner, and Ballman in 1967 to measure the elastic constants of Bismuth Germanium Oxide (BGO). In both BGO studies, the crystal plates were assumed infinite in both transverse dimensions. [Ref. 18:2] With this refined technique Slobodnik and Sethares succeeded in accurately determining the elastic constants of BGO.

The Slobodnik and Sethares study clearly demonstrated the advantages in using a special crystal holder, a Wayne-Kerr VHF admittance bridge, and a spectrum analyzer. These three pieces of equipment allowed greater experimental accuracy, precision, and sample purity. The use of a special crystal holder, or "jig" was advantageous since a transducer did not have to be cemented onto the crystal, nor did a buffer rod have to be prepared. The detected resonant frequencies were thus only due to the BGO alone. The Wayne-Kerr VHF admittance bridge was advantageous in that it could easily be adjusted to produce resonance and resonant frequencies in the crystal. The spectrum analyzer was advantageous in that it produced an easy visual check to determine where the resonant frequencies of the crystal occurred. For these reasons, the adopted technique in this InP research adopted some of the equipment and methods used in the 1971 Slobodnik and Sethares study.

Similarly in 1981, Melcher, Schickfus, and Baumann refined a simple

set of circuits for measuring the elastic constants of Z-cut quartz. This circuitry had been previously developed by Melcher, Bolef, and Merry in 1968 to measure the elastic constants of (antiferromagnetic) Rubidium Magnesium Fluoride ($RbMnF_3$). This technique was capable of automation and accuracy of one part per 10^8 or better. [Ref. 14:432]

In 1981 Melcher study clearly demonstrated the advantages of circuitry with lock-in capabilities, low power requirements, and high precision. The lock-in circuitry was advantageous since the resonant frequency was able to be determined to the tenths of Hz. Thus resolution was better than 3×10^{-8} for the sample. [Ref. 14:433] In addition, precision did not depend on the human eye detecting the resonant frequency. The advantage of low power was desirous since the system could measure frequency changes without heating or cooling the sample. Thus the environmental temperatures registered by a thermometer would be equal to the temperature of the sample. For these reasons, the new technique in this InP research adopted some of the equipment and methods used in the 1981 Melcher, Schickfus, and Baumann study.

This research on InP therefore combines these two techniques, employing the theory developed by Tiersten. The resulting circuitry combination uses common laboratory equipment designed to produce accurate, reproducible, and pure values of the elastic constants of InP. The InP technique utilizes the special crystal holder, Wayne-Kerr bridge, and spectrum analyzer of the 1971 Slobodnik and Sethares study. This equipment is supplemented with an environmental chamber and thermometer to respectively change and record the environmental temperature of the InP crystal. The InP technique also utilizes the lock-in amplifier, oscillo-

scope, signal generator, and the principles of integration and addition of the 1981 Melcher study. This equipment and principles are supplemented with an enable/disable switch, amplifiers, and a blocking capacitor that respectively allow automation of the system, amplification of a weak acoustic signal, and the minimizing of system noise. In addition, an analog integrator and adder were constructed from operational amplifiers and resistors to allow precise lock-in. A complete list of the equipment used in this study is listed in Appendix B. However, in order to understand why the system was designed this way and how it works, it is important to first discuss the remaining major forecasted characteristics of the InP crystals.

Desired Characteristics of the InP Crystals

Since time was an important factor in this InP research, the crystals were prepared to exact and demanding specifications so that an acoustic response could be detected. Since the Air Force Institute of Technology (AFIT) and RADC were unable to prepare the crystals for measurement, the work was contracted out. The company that performed the orientation, cutting, and polishing of the InP crystals was Interactive Radiation Incorporated (INRAD). A detailed list of the specifications for crystal preparation is described in Appendix C.

Assuming the InP crystals met the specifications as discussed in Appendix C, they would have several noteworthy characteristics. First, they would be small. With twinning having occurred in one of the boules, it was reasonable to expect samples of the size 4 mm x 5 mm x 1 mm thick. INRAD would try to produce 3 thick plates of 11 mm x 10 mm x 5 mm thickness in size, but the majority of the crystals would be small.

Second, the InP crystals would be single crystal. For if the InP sample was not all one crystal, no acoustic responses would be able to be detected. Anything but single crystal InP would cause severe attenuation of the acoustic wave especially at the interfaces of the crystal boundaries within the InP sample. Therefore in order to minimize attenuation and dispersion, the InP had to be single crystal.

Third, the InP crystals would be semi-insulating. The expected resistance of the InP would exceed 10^7 ohm-cm. If the InP did not have sufficiently high resistance, severe attenuation of the acoustic signal would occur causing the return signal to be either too weak to be detected or nonexistent. Therefore, in order to minimize attenuation, the InP had to be semi-insulating. Furthermore, the crystal had to be semi-insulating in order to use its intrinsic piezoelectricity to launch the acoustic waves.

Fourth, the InP crystals would have good polish and parallelism. Without good polish ($\pm$ 1500 angstroms), the propagating wave would not be reflected coherently. Thus the return signal would either be too weak to be detected or nonexistent. Needless to say, the InP crystals had to be free of large pits and scratches. Without good parallelism the reflected waves would destructively interfere, causing a loss in the resonator Q of the InP crystals. Poor parallelism would also cause air gaps to form between the crystal and the crystal holder, and therefore severely attenuate any travelling waves. Thus, in order to maximize resonator Q, and signal strength, and to minimize dispersion, propagation loss, and attenuation, the crystals had to have good polish and parallelism.

Fifth, the InP crystals would have to be properly oriented. If they were not properly oriented ($\pm$ 0.2 degrees), then pure modes of vibration would not occur and the theories discussed in Section II-1 would not be applicable to this research.

These are the five major characteristics desired for the InP crystals. If they all held true, the new technique would detect an acoustic response in the InP. From detection of an acoustic response, Δf_{HH} could then be calculated and subsequently the elastic constants of InP. The details of how the system detects an acoustic response are explained in the next chapter.

III. Description of Test System and Data Collection

Theory of Test System

Assuming that the InP crystals would meet the specifications given to the contractor, the theory to measure the acoustic responses is very simple. Recalling that the system must measure Δf_{HH}, the change in the high harmonic resonant frequencies, the problem simplifies to the ability of the system to locate precisely the peaks of the resonant frequencies. A typical signal response of a resonance curve is illustrated in Figure III-1. Here the resonant frequency produces the highest value of the resonance curve.

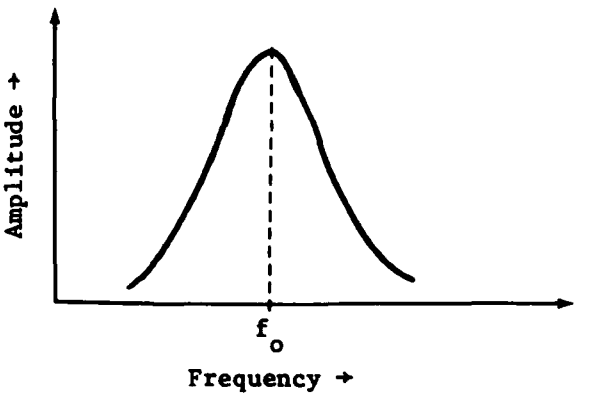

Figure III-1. Typical response of signal strength versus frequency at resonance.

If the system had an RF carrier frequency, f_{cw}, which was frequency modulated (FM) at an audio frequency, f_A, centered at f_{cw}, the carrier signal would be amplitude modulated (AM) at the receiver at the frequency f_A by an amount proportional to the slope of the resonance at f_{cw}. [Ref 13: 1619] If there existed some sort of lock-in device referenced to f_A, its output would be proportional to the first derivative of the

resonance curve's envelope. At $f_{cw} = f_o$ the slope of the resonance curve is zero, hence its first derivative and the output of the lock-in device are both zero. Thus, the amplitude modulation resulting when f_{cw} is tuned off the center of the resonant frequency is shown schematically in Figure III-2a. When f_{cw} is tuned to $f_{cw} = f_o$, as shown in Figure III-2b, no amplitude modulation at f_A results, but some amplitude modulation will occur at $2f_A$ and at higher harmonics. The lock-in device must therefore reject all signals not at f_A in addition to a null reading when $f_{cw} = f_o$. Therefore, detection is possible since this null condition is quite sharp even for rather highly attenuating samples (ie: low Q). [Ref. 13: 1619] Thus for this InP research, detection of the precise resonant frequency peaks is possible given the samples are properly prepared. The problem now simplifies to building a system that precisely locks onto the resonant frequencies. This is discussed in detail in Section III-2.

Description of Test System

The block diagram of this InP experimental system is shown in Figure III-3. An RF CW oscillator with a DC coupled FM input, the Hewlett-Packard (HP) 8654A Signal Generator, is modulated by the audio oscillator of a Princeton Applied Research (PAR) 184 Lock-In Amplifier. The CW oscillator is used to generate the carrier frequency, f_{cw}. The PAR amplifier is used to provide a sweeping frequency, f_A, and is fine tuned by a feedback loop. The output of the CW oscillator is inputed to the source connector of the Wayne-Kerr (WK) bridge, and also to a frequency counter, the HP 5340A Electronic Frequency Counter. The WK

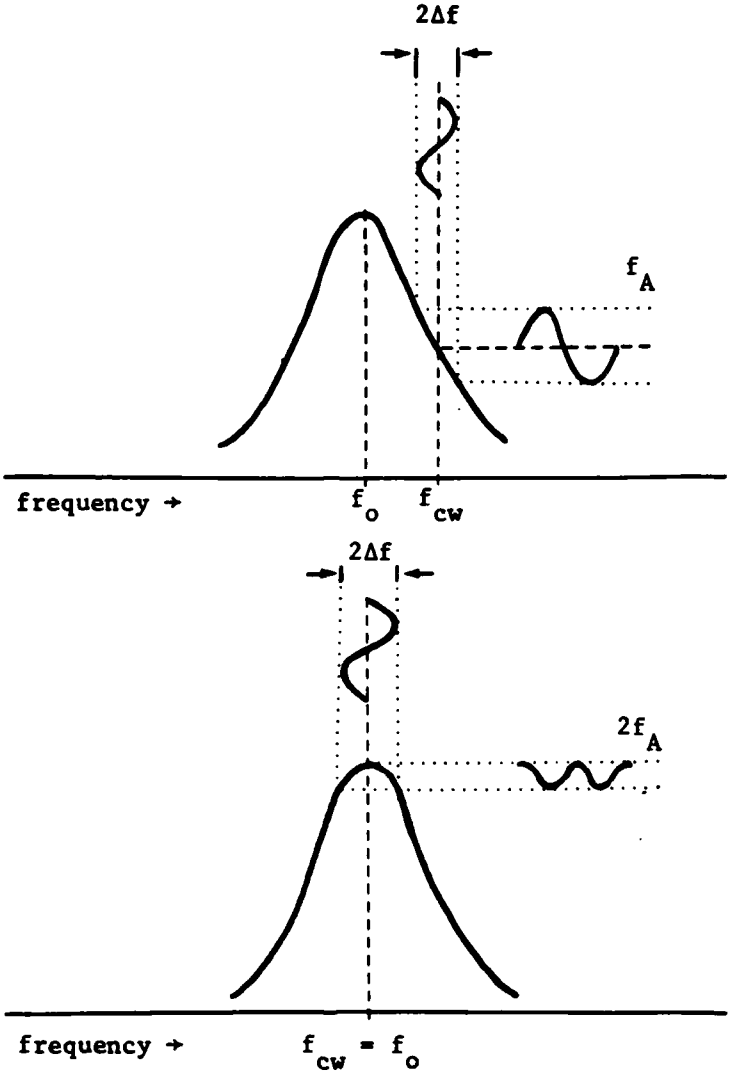

Figure III-2. Schematic diagram of the effect of FM deviation $2\Delta f$ centered at the carrier frequency f_{cw}. The audio modulation is f_A. The resonant frequency is f_o. In Figure 2a, $f_{cw} \neq f_o$ results in amplitude modulation of the carrier signal at the audio frequency f_A. Nulling of this amplitude modulation is shown in Figure 2b. By precise adjustment of the carrier frequency such that $f_{cw} = f_o$, the output has some modulation at $2f_A$ (and higher harmonics), but none at f_A. Since the lock-in amplifier rejects all signals not at f_A, it indicates a null reading at $f_{cw} = f_o$.

Bridge is used to balance the reactance of the InP crystal near its reso-

nant frequency and cause the crystal to produce a strong signal at its

resonant frequency for detection. The frequency counter continuously monitors the frequency of the CW oscillator and will provide the exact resonant frequency. The two test point terminals of the WK bridge are connected to the ends of the crystal holder which will contain the InP crystal. The crystal holder is placed within the environmental chamber, the Tenney Jr. Environmental Chamber, and its environmental temperature is monitored by a thermometer, a Cyborg Thermal P-642 Audio Thermometer. Thus the environmental temperature of the InP crystal can be varied and monitored to within $\pm$ 0.01 °C. The output of the WK bridge is passed through two amplifiers in series, a Watkins-Johnson Cascade Amplifier, and a HP 8447A Amplifier, in order to boost up the detected signal. From the amplifiers the signal is inputed into a spectrum analyzer, a Tektronix 7603 Spectrum Analyzer, in order to provide a visual check for the resonant frequencies, and a HP 962B Crystal Detector which detects the envelope of the amplified signal. From the envelope detector the detected signal is inputed to a DC blocking capacitor located on the Elite-3 Wiring Board. From the DC capacitor the detected signal is amplified and then compared to the original by an analog adder inside the PAR lock-in amplifier. The difference between the two signals is integrated by an analog integrator. The integrator is constructed of operational amplifiers and resistors and provides a dc correcting voltage. This voltage is then added to the sweeping frequency of the PAR amplifier by an analog adder. This sum is inputed back to the DC coupled FM input of the CW oscillator completing the feedback loop.

The system accomplishes theory as discussed in Section III-1 in the following manner. The CW oscillator provides a f_{cw} which is frequency

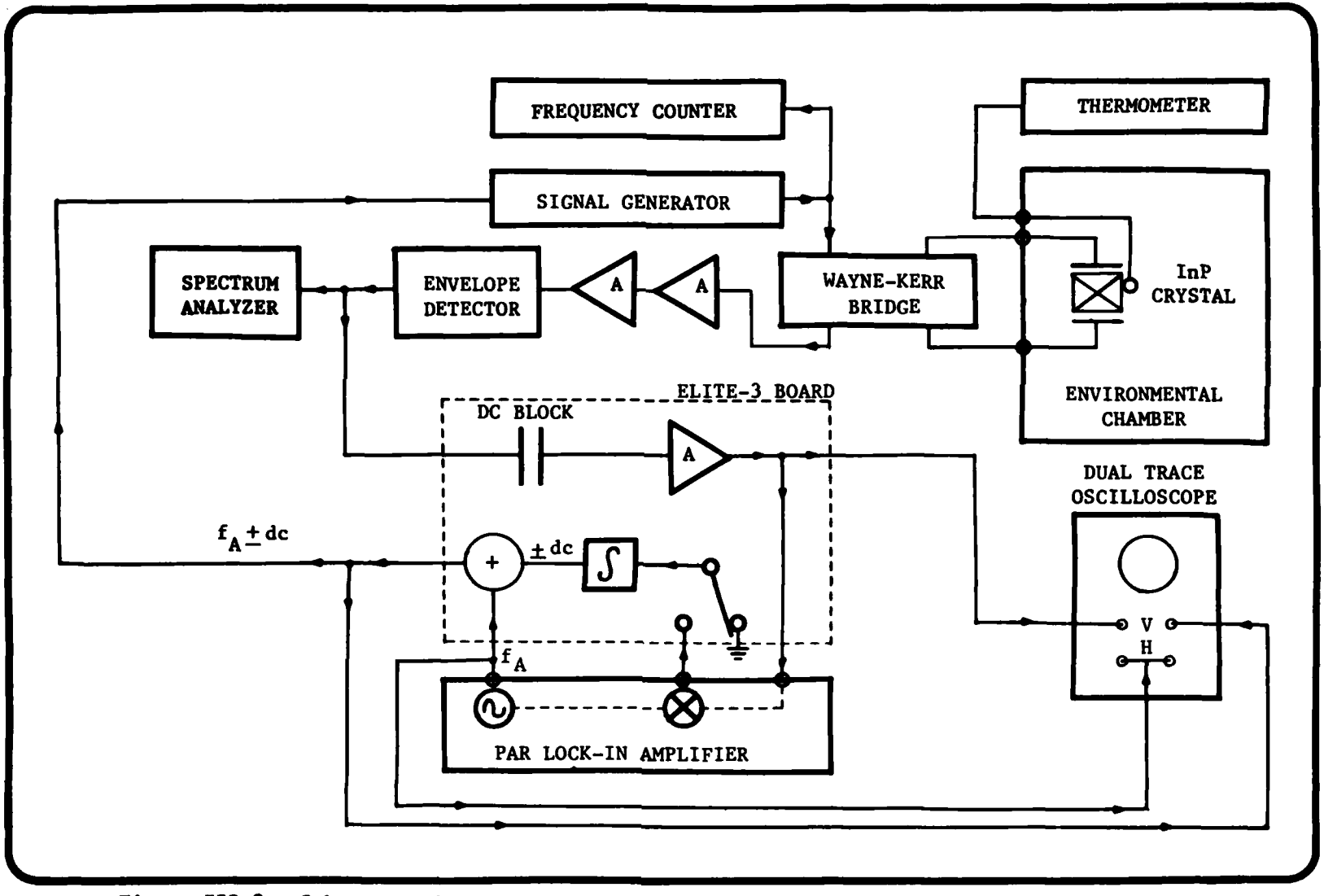

Figure III-3. Schematic Block Diagram of InP Test System to measure resonant frequencies.

modulated by f_A that is produced by the PAR amplifier. This modulation, f_A, causes f_{cw} to be swept across the resonance curve and f_o. This sweeping of f_{cw} produces an AM signal at the output of the WK bridge. The AM signal has frequency f_A if $f_{cw} \neq f_o$. If $f_{cw} = f_o$, the AM signal has frequency $2f_A$ and higher harmonics. For this case of $f_{cw} \neq f_o$, there exists no f_A component in the AM signal. Continuing with the case $f_{cw} \neq f_o$, the first adder located in the PAR amplifier subtracts the frequency of the AM signal from the original sweep frequency, f_A. The difference is integrated providing a dc voltage proportional to the frequency difference $f_o - f_{cw}$. When the enable switch is on, this dc voltage is added to the original sweep frequency. This signal becomes an input to the DC coupled input of the CW oscillator causing f_{cw} to move toward f_o and lock onto f_o. The key to lock-in is the feedback loop. If $f_{cw} > f_o$, the integrator outputs a negative dc voltage decreasing f_{cw}. If $f_{cw} < f_o$, the integrator outputs a positive dc voltage increasing f_{cw}. Thus f_{cw} is able to lock onto f_o precisely.

The important modification to the feedback loop from the 1981 Melcher study is the use of an external analog integrator. The result, however, is the same as the 1981 Melcher study. The output of this integrator is added to the audio output of the PAR amplifier and thus a feedback loop is formed which corrects f_{cw} until $f_{cw} = f_o$. This system is an automatic fine tuning system that locks f_{cw} onto f_o. Long integration times of the frequency counter can be used to increase the resolution of the resonant frequency to the tenths of Hz. Also the counter may be connected to a calculator for automatic data acquisition and further data processing. The hook ups to the oscilloscope provide an additional visual

check for coarse tuning to the resonant frequency, f_o. The spectrum analyzer provides the primary visual check for coarse tuning to the resonant frequency. The oscilloscope can also be used to monitor the stability of the system. In this InP research both the spectrum analyzer and the oscilloscope were used to provide visual checks for resonance.

Some minor modifications were also made to provide additional stability and control of the InP system. The first modification concerns stabilizing and maximizing the signal to noise ratio (SNR) to the PAR amplifier and oscilloscope. From the output of the envelope detector, the HP 962B, a DC blocking capacitor, 2μF, was used to maximize the SNR of the detected signal by minimizing the low frequency noise entering the system. From the DC capacitor the signal passed through a 100 to 1 voltage divider in order to scale down the signal strength for the PAR amplifier. This was done since the PAR amplifier was very sensitive. The PAR amplifier's lowest A/V setting, equal to 10^{-5}, was more than adequate to detect the AM signal. From the voltage divider the signal passes through a low pass filter and a variable gain amplifier. This maximizes the SNR of the signal prior to its input to the oscilloscope which also provides an additional visual check for detected resonance. This circuitry is illustrated in Figure III-4.

The second mofification concerns filtering out noise from the power supply to the operational amplifiers. This is important since the operational amplifiers are the basis of the analog integrator and adder in the feedback loop. Therefore, in order to maintain a constant 30 volt difference in the power supply, the +15V, -15V, ground, and common

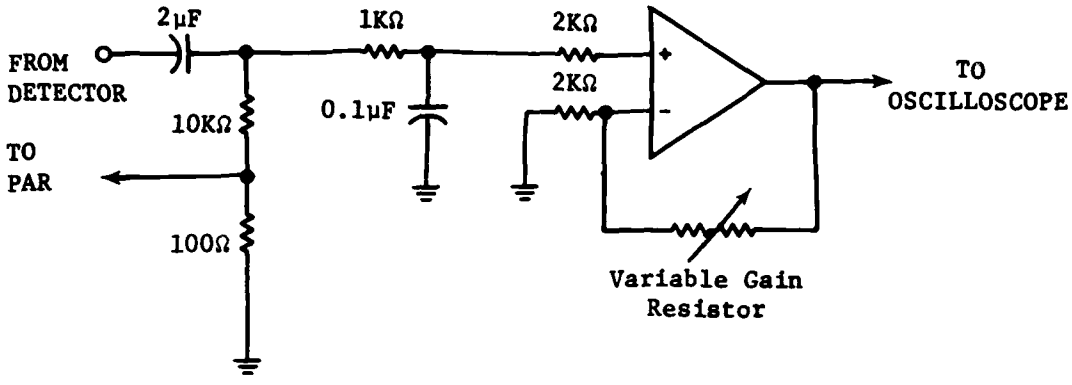

Figure III-4. Schematic diagram of detailed circuitry for adjustment of input signal to oscilloscope.

terminals of the power supply, the HP 6236B, were connected via a power filter. This power filter is constructed of two 2μF capacitors, and is illustrated in Figure III-5.

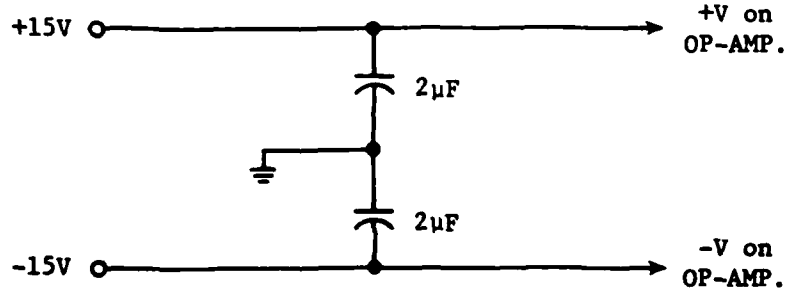

Figure III-5. Schematic diagram of power filter.

The third modification concerns the analog integrator. In addition to an enable/disable switch, this circuit includes a dc voltage level

adjuster. The purpose of the enable/disable switch is obvious. When feedback is desired, the switch is enabled, allowing the output of the "function out" terminal of the PAR amplifier to be integrated and thus provide the dc correcting voltage. The output of the "function out" terminal of the PAR amplifier is the output of the adder which compared the frequency of the detected signal with that of the original sweeping signal. When feedback is not desired, the switch is disabled. Since the disable terminal is tied to ground, no correcting voltage comes from the integrator. The DC level adjuster provides enough gain into the feedback loop so that lock-in is within the limits of the correcting voltage of the integrator. The DC level adjuster consists of two inverting operational amplifiers, one of which has a variable gain control. This set of circuitry is illustrated in Figure III-6. For correct initialization, the output of the DC Level adjuster should be zero when the output from the "function out" terminal of the PAR amplifier is zero.

These are the details of the feedback control loop. In short, the stable operation of the feedback loop is necessary for the precision required of the InP experimental system. Stability is maintained by such circuitry as the filters, voltage divider, enable switch, power filter, and variable gain amplifiers. In addition to monitoring by the oscilloscope, stability is also maintained by proper adjustment of all the various time constants. There exist four important time constants in the InP system. The first is τ_S, the characteristic time constant of the sample, where $\tau_S = Q/\pi f_o$. The second is τ_A, the modulation period of the sweeping frequency, where $\tau_A = 1/f_A$. The third is τ_{int}, the in-

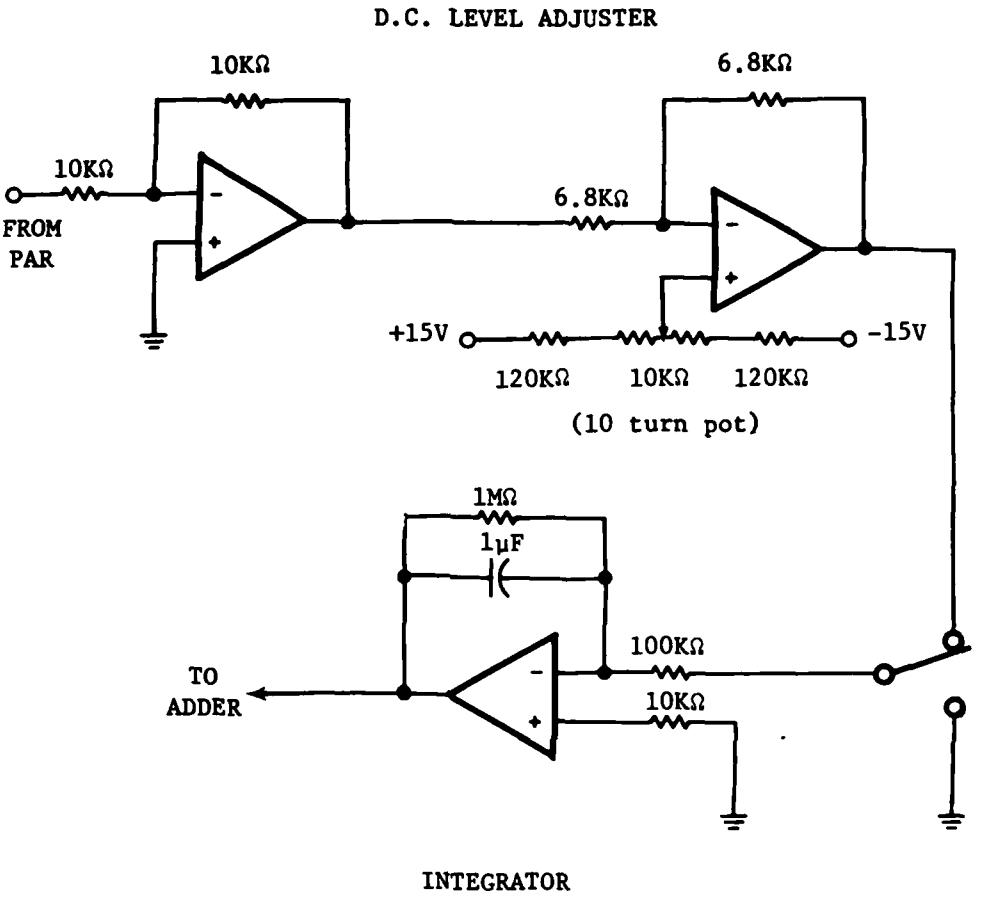

Figure III-6. Schematic diagram for the control system of the analog integrator in the feedback loop.

tegrator time constant, where $\tau_{int} = R_{int} C_{int}$ (1 sec. in this case). The fourth is τ_{PAR}, the PAR amplifier filter time constant. The requirements for stability and precision dictate $\tau_{int} >> \tau_{PAR}$, $\tau_{int} >> \tau_S$, and $\tau_A >> \tau_S$. [Ref. 13: 432] Proper adjustment of these four variables allows greater precision since all four can be adjusted as desired to prevent beating or excessive delay and maintain stability.

This is the system used to measure the relative changes in the

resonant frequencies of InP. Figure III-3 gives the general schematic diagram of the system. Figure III-4, III-5, and III-6 describe important details of the InP system. Appendix B gives the complete equipment list. For a detailed description and picture of the crystal holder, the interested reader should refer to Slobodnik and Sethares, 1971. The crystal holder used in this InP research is the same one used in the 1971 Slobodnik and Sethares study. [Ref. 18]

Experimental Procedure

The first task of the experimental procedure was to check if the system worked. An X-cut quartz sample was prepared by Valpey Fisher Corp. (VFC) with gold leads evaporated onto the quartz. The quartz was then placed in the environmental chamber and connected to the input terminals of the WK bridge by a cable passing through the walls of the chamber. Using an f_o = 30 MHz, the Q factor was approximately 51,000. τ of the counter was set to 1 second, f_A to 900 Hz, and τ_{PAR} to 100 milliseconds. This was to insure $\tau_A >> \tau_S$, $\tau_{int} >> \tau_S$, and $\tau_{int} >> \tau_{PAR}$. Resonance was thus detected to the ones of Hz. Velocity measurements were accurate to within 0.5% of the known results. X-cut quartz is known to have a temperature dependence of -20 to -24 ppm per °C. The system measured -19.5 ppm per °C. The measured temperature dependence was thus within 1 ppm per °C of the known results.

Now that the system had been carefully checked out with both theory and quartz and found to be accurate, the remaining task left was to measure Δf_{InP} for the InP samples. The InP samples returned by INRAD totalled eleven. Six were small plates, three were thick plates, and two were irregular plates. See Appendix C for details of orientation

and preparation. Thus the required number of samples had been manufactured. The second task was to see if the crystals were up to the desired specifications.

The easiest way to perform the second task and assess its impact was to first see if resonance could be detected on the InP crystals. Unfortunately, resonance was not detected on any of the INRAD prepared samples. Resonance detection was attempted three different ways with the InP samples.

The first way involved parallel excitation along the longer major face edge. This involved placing the crystals snuggly within the crystal holder with the longer face dimension flat against the edges of the crystal holder. No resonance was detected by this method for all the InP samples.

The second way involved parallel excitation along the smaller major face edge. This involved rotating the crystal 90° along the horizontal axis from the previous method. In this case the smaller dimension was placed flat against the edges of the crystal holder. No resonance was detected by this method for all the InP samples.

The third way involved perpendicular excitation. This method only involved four of the InP samples. For this method silver was evaporated on the major faces of the InP samples and leads were attached with silver epoxy. The leads were then directly connected to the input terminals of the WK bridge. No resonance was detected by this method for all the InP samples tested. The thickness of silver evaporated onto the InP was 0.33 microns.

With resonance unable to be detected by the system on the InP

samples, the next task was to examine specific characteristics of the InP samples, characterize these traits, and design an alternate procedure to successfully detect the resonant frequencies of the InP.

There were many areas of crystal preparation that could have been in error. After discussions with various scientists from RADC and the Massachusetts Institute of Technology (MIT) Lincoln Lexington Laboratories, the major areas investigated were purity, resistivity, polish, surface roughness, parallelism, and crystal structure of the InP crystals. Fortunately, additional InP crystals were donated during this time period from RADC/ESM (Boule #3) to be used as a comparison and reference to the original set of InP crystals (Boule #1 and Boule #2). Since various tests used to measure these InP characteristics apply to more than one area of concern, documentation of this InP investigation will be structured by topic.

The first area of investigation concerned purity. Detailed studies were made of the histories of the InP samples. A review of RADC documentation revealed that the InP seed crystals were directly synthesized from the elements. It also showed that it was some of the purest InP produced by RADC. In the growing of the boules, however, it was discovered that Boule #1 had been overdoped with iron (Fe). As previously mentioned, Boule #2 had twinned due to its low concentrations of Fe and dislocation densities. Suspecting that the boules could have significant differences in purity, transmission infrared photographs were taken of various InP samples from both Boule #1 and Boule #2. The photographs verified that all but one of the InP samples from Boule #1 were of insufficient purity and contained too much Fe. Photographs of the InP

samples from Boule #2, however, indicated that these crystals may be of sufficient purity. Infrared photographs were also taken of the Boule #3 InP samples which were known to be of high purity. Photographs of these samples matched those taken of Boule #2. Therefore, concerning purity, it was reasonable to assume that Boule #1 had lower purity than Boule #2, and that Boule #2 and Boule #3 had sufficiently high purity.

The second area of investigation concerned resistivity. Resistivity was measured by three different tests. The first test measured surface resistivity by a Micromanipulator Digital Resistivity Test System (4 point probe). Two categories of InP samples evolved from this test. InP samples with a short circuit reading on the probe indicated low resistivity. InP samples with an open circuit reading on the probe indicated high resistivity. The Boule #3 InP samples were known to have high resistivity, and as expected, the probe registered open circuit readings for all these samples. Only four of the original samples registered open circuit readings. All four samples were from Boule #2. These crystals were labelled SP #12, SP #32, TP #22, TP #32. The first reference number refers to the plate orientation and the second number refers to the boule source. Thus, SP #12 is an InP small plate of <111> orientation from Boule #2. SP #32 is an InP small plate of <100> orientation from Boule #2. TP #22 is an InP thick plate of <110> orientation from Boule #2. TP #32 is an InP thick plate of <100> orientation from Boule #2. These were the only samples from Boules #1 and #2 that registered high surface resistivity.

The second test measured bulk resistivity by infrared photography. Various InP samples from all three boules were examined by infrared

photography. The results confirmed that the samples from Boule #1 were of low bulk resistivity while samples from Boule #2 and Boule #3 were of high bulk resistivity.

The third test measured bulk resistivity by a highly sensitive ohmmeter. Various InP samples from all three boules had silver (Ag) evaporated onto their major faces. Leads were then attached with silver paint and connected to the terminals of the ohmmeter and resistivity readings were taken. Resistivity readings from Boule #1 samples were approximately 13.0 Ω. Resistivity readings from Boule #2 samples were approximately 1.5×10^7 Ω. Resistivity readings from Boule #3 samples were approximately 1.0×10^7 Ω. The results confirmed that the samples from Boule #1 were of low bulk resistivity while the samples from Boule #2 and Boule #3 were of high bulk resistivity. Thus all three tests were in agreement indicating that only 4 Boule #2 samples and all of the Boule #3 samples were of sufficiently high resistivity.

The third area of investigation concerned polish and surface roughness. Polish and surface roughness were examined by three different methods. The first test involved examination by optical microscope. Various magnifications up to 320X were used to check for large pits or scratches on the major faces. All InP samples showed no signs of large pits or scratches. The second test involved examination by Scanning Electron Microscope (SEM). Various SEM magnifications up to 5800X were used to check for pits, small knicks, or grooves. SEM examinations showed that the Boule #1 and Boule #2 INRAD polished samples were much smoother and better polished than the Boule #3 RADC polished samples by several orders of magnitude. The third test involved examination by a

Sloan Dektak Surface Profile Measuring System (Dektak). Various InP samples from all three boules were examined under the Dektak system. Results of the examination confirmed that all the INRAD samples were several orders of magnitude smoother and better polished than the RADC samples.

The fourth area of investigation concerned parallelism. Parallelism was examined by three different tests. The first test involved examination by micrometer and optical microscope. For examination by micrometer, the crystals were measured to compare the physical dimensions to the specifications of Appendix C and serve as a reference base for the parallelism tests. All three thick plates measured 11.006 mm x 9.955 mm x 4.970 mm. All the small plates measured 4.960 mm ($\pm$ 0.005 mm) x 3.960 mm ($\pm$ 0.015 mm) x 1.026 mm ($\pm$ 0.003 mm). All these measurements demonstrated that the length, width, and thickness of the crystals were within tolerance of the specifications. For examination by optical microscope, various magnifications up to 160X were used to investigate edge definition and parallelism of the 4 minor faces of the InP samples. In the area of edge definition, the INRAD samples were cut several orders of magnitude better than the RADC samples. Parallelism of the minor faces also was several orders of magnitude better for the INRAD samples than the RADC samples. The second test involved examination by SEM. Various magnifications up to 5800X were used to investigate parallelism and edge definition. The results showed the INRAD samples to be several orders of magnitude better than the RADC samples. The third test involved examination by the Dektak system. In parallelism of the major faces, all INRAD samples were at least 100X better than the

RADC samples. Thus all three tests were in agreement indicating that all INRAD prepared samples had sufficient polish and surface smoothness. The RADC prepared samples, however, did not have sufficient polish and surface smoothness to be used in the original InP measuring system. (Refer to Appendix E.)

The fifth area of investigation concerned the crystal structure of the InP samples. Crystal structure was examined by infrared photography. Although the results of the examination are not definitive, close investigation revealed threads of precipitated Fe interspersed throughout the crystal. If these threads are single crystal material, it is reasonable to assume that they are of different crystal type and orientation relative to the desired InP single crystal.

These five areas of investigation revealed several major traits of the InP samples. A definite difference existed in the INRAD prepared samples depending on the boule source. Although all these samples had good polish, surface smoothness, and parallelism, Boule #1 had poor resistivity and purity, while Boule #2 had good resistivity and purity. The RADC prepared InP samples, however, were not suitable replacements for the INRAD prepared samples. Even though they had high resistivity and purity, their polish, surface roughness, and parallelism were poor. Taking into account these major characteristics and the plate orientations needed to derive the elastic constants of InP, an alternate technique to experimentally determine the elastic constants was required. There were two possible methods. The first method involved increasing the sensitivity of the original InP measuring system by impedance matching and using high input impedance equipment. This was too complex

a solution and was thus discarded. The second method was to use the original InP measuring system, but to discard the special crystal holder and cement a piezoelectric transducer onto the InP. This was the simplest solution and the easiest one to implement within the time constraints of this research and the new limitations of the INRAD prepared InP crystals. However, in order to understand this modified alternate technique, its theoretical basis must first be explained.

Modified Measurement Technique for InP

Since the crystals did not meet their specifications, the measurement technique required some modification. Since the resistivity was very low on half of the INRAD polished InP samples, the alternate technique had to incorporate measuring acoustic responses in conducting InP. Thus, in this case, a piezoelectric transducer was cemented onto the InP crystal. Even though some of the InP crystals were conducting, piezoelectric excitation could still be used if the transducer was piezoelectric. As recommended by McSkimin, X-cut quartz was used as a transducer to excite longitudinal waves, and Y-cut quartz was used to excite shear waves. The main assumption in using this technique was that the quartz transducer is strong enough acoustically to excite the InP which was not able to be excited on its own. Thus the modified technique takes into account the new limitations of the InP crystals found in Section III-3. From the measured resonant frequencies of the combination, the coupling effects of the transducer were calculated out, and the resonant frequencies of the InP were determined. Because quartz transducers have a relatively low loss [Ref. 11: 306], this alternate

method worked even though the primary technique was unable to detect any acoustic resonances.

Theory for Modified Technique

In order to derive the necessary relations for the change in resonant frequencies and velocity, consider the transmission line model, as illustrated in Figure III-7.

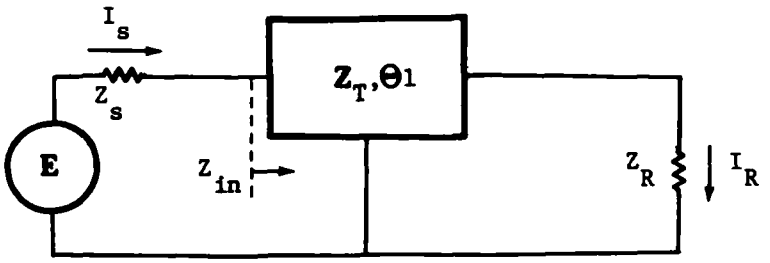

Figure III-7. Equivalent circuit for a section of transmission line with input and output terminals. [Ref. 11: 277]

The form for the differential equation of motion for the transmission of travelling waves in the simple unidirectional case turns out to be similar to the form for electrical waves travelling along an electrical transmission line. [Ref. 11: 276] Applying the basic form of the transmission line model, the input impedance to the InP crystal, Z_{in}, is then:

$$Z_{in} = Z_T \left\{ \frac{Z_T \sinh\theta l + Z_R \cosh\theta l}{Z_T \cosh\theta l + Z_R \sinh\theta l} \right\} \qquad (3\text{-}1)$$

where Z_T is the characteristic impedance of the transmission medium, l is the length of the transmission medium, θ is the propagation constant,

and Z_R is the terminating impedance of the transmission medium.

Setting $Z_R = 0$, causing the medium to be terminated in a short, results in:

$$Z_{in} = Z_T \tanh\theta l \tag{3-2}$$

The propagation constant, θ, can be expressed in terms of its complex coefficients, A, the attenuation, and B, the phase shift, such that:

$$\theta = A + jB \tag{3-3}$$

where

$$B = \frac{\omega}{v} \tag{3-4}$$

Equation 3-2 then becomes:

$$Z_{in} = Z_T \left\{ \frac{(\tanh Al)(1+\tan^2 Bl) + j(\tan Bl)(1-\tanh^2 Al)}{1 + \tanh^2 Al \cdot \tan^2 Bl} \right\} \tag{3-5}$$

Assuming that A, the attenuation, and B, the phase shift, are very small, then $\tan Bl \ll 1$ and $\tanh^2 Al \ll 1$, $\tan^2 Bl \approx 0$, and $\tanh Al \approx Al$. By the transmission line model, Z_T may be replaced with ρva. Equation 3-5 then becomes:

$$Z_{in} = \rho va Al + j\rho va \tan Bl \tag{3-6}$$

where ρ is the density of InP, v is the velocity of propagation in the crystal, and a is the cross section area of the crystal. Equation 3-6 can be approximated at frequencies near the resonant frequency of the combination by an equivalent circuit consisting of resistors, capacitors, and inductors in series. [Ref. 10: 307] This is illustrated in Figure

III-8.

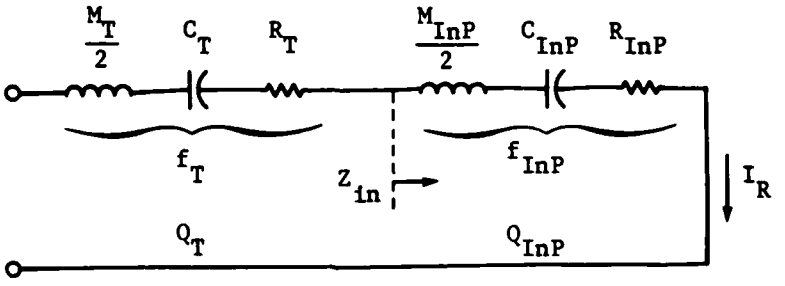

Figure III-8. Equivalent circuit for a piezoelectric transducer attached to an InP single crystal.

To see that ρvaAl is indeed the real part of Z_{in} and non-zero, the transmission line model is applied to the Q of the InP crystal. From Figure III-8, defining Q_{InP} equal to the Q of the electrical circuit results in:

$$Q_{InP} = \frac{M_{InP}\omega}{2R_{InP}} \tag{3-7}$$

where M_{InP} is the mass of the crystal, ω is the resonant frequency of the crystal in radians, and R_{InP} is the electrical resistance of the crystal. Q_{InP}, however, is also the inverse of the internal friction of the crystal. Since the internal friction of a travelling sinusoidal wave in a crystal is related to the stresses and strains caused in the crystal, applying Hooke's Law to this sinusoidal motion results in:

$$Q_{InP} = \frac{B^2 - A^2}{2AB} \approx \frac{B}{2A} \quad \text{for } B>10A \tag{3-8}$$

This equation would hold true for plane wave propagation in both longi-

tudinal and shear waves.

Equating the two expressions for Q_{InP} to each other, results in:

$$A = \frac{2BR_{InP}}{2M_{InP}\omega} = \frac{BR_{InP}}{M_{InP}\omega} \qquad (3\text{-}9)$$

Therefore:

$$\rho vaAl = \frac{\rho vaBR_{InP}l}{M_{InP}\omega} = \frac{(\rho al)R_{InP}B}{M_{InP}(\omega/v)} \qquad (3\text{-}10)$$

but,

$$\rho al = M_{InP} \qquad (3\text{-}11)$$

and

$$B = \frac{\omega}{v} \qquad (3\text{-}12)$$

Thus,

$$\rho vaAl = R_{InP} \qquad (3\text{-}13)$$

At resonance $\rho vatanBl$ becomes indeterminate (infinity) and similarly, so does $tanBl$. Therefore:

$$Bl = \frac{n\pi}{2} \quad (n \text{ is odd integer}) \qquad (3\text{-}14)$$

Setting $n = 1$ and substituting equation 3-9 into equation 3-14 results in:

$$\frac{M_{InP}\omega Al}{R_{InP}} = \frac{\pi}{2} \qquad (3\text{-}15)$$

or:

$$\omega = \frac{\pi R_{InP}}{2M_{InP}Al} \tag{3-16}$$

where $\omega = 2\pi f$. Therefore:

$$f = \frac{\pi R_{InP}}{2M_{InP}Al2\pi} \tag{3-17}$$

or:

$$f = \frac{R_{InP}}{4M_{InP}Al} \tag{3-18}$$

Noting that the impedances of the crystal and transducer are in series, and applying the linear model of electrical circuits, the expression for Z_C, the impedance of the transducer-InP combination is then:

$$Z_C = Z_{InP} + Z_T \tag{3-19}$$

where Z_{InP} is the impedance of the InP crystal, and Z_T is the impedance of the transducer. Applying equation 3-13 and recalling that Z can be expressed as ρva, results in:

$$\frac{R_C}{A_C l_C} = \frac{R_{InP}}{A_{InP} l_{InP}} + \frac{R_T}{A_T l_T} \tag{3-20}$$

Dividing the left and right hand sides by 4, and multiplying each term, top and bottom, in equation 3-20 by their respective masses, the result is:

$$\frac{M_C R_C}{4M_C A_C l_C} = \frac{M_{InP} R_{InP}}{4M_{InP} A_{InP} l_{InP}} + \frac{M_T R_T}{4M_T A_T l_T} \tag{3-21}$$

Applying equation 3-18 to equation 3-21 results in:

$$M_C f_C = M_{InP} f_{InP} + M_T f_T \tag{3-22}$$

Applying equation 3-19 to equation 3-22 then results in:

$$f_C(M_{InP} + M_T) = M_{InP} f_{InP} + M_T f_T \tag{3-23}$$

Solving for f_{InP} gives:

$$M_{InP} f_{InP} = M_{InP} f_C + M_T f_C - M_T f_T \tag{3-24}$$

$$= M_{InP} f_C + M_T (f_C - f_T) \tag{3-25}$$

or:

$$f_{InP} = f_C + \frac{M_T}{M_{InP}} (f_C - f_T) \tag{3-26}$$

Measuring f_C for two successive frequencies at high harmonics at the same temperature results in:

$$\Delta f_{InP} = \Delta f_C + \left\{ \frac{M_T}{M_{InP}} \cdot \Delta f_C \right\} \tag{3-27}$$

$$= \Delta f_C \left[1 + \frac{M_T}{M_{InP}} \right] \tag{3-28}$$

where Δf_C is the change in higher harmonic frequencies for the quartz-InP combination, and Δf_{InP} is the change in higher harmonic frequencies for a pure InP single crystal. Since in this case there are many resonances of InP for each resonance of the transducer, $f_{T_1} - f_{T_2} = 0$ when considering Δf_C. Therefore by knowing the change in frequencies of the high harmonics of the transducer-InP combination and knowing the masses of the resonating transducer and InP crystal volumes, the actual

value of the change in the higher harmonics for InP can be calculated. It should be noted that if the InP crystal does not have the same cross sectional area as the transducer, the ratio of the weights of the transducer and InP crystal is not equal to the ratio of their masses.

Thus, if the modified technique were to be applied, first Δf_C would have to be measured. Second, Δf_{InP} would be computed knowing Δf_C, M_{InP}, and M_T. Third, Δf_{InP} would be set to Δf_{HH} for reasons previously discussed in Section II-1. Finally, the elastic constants of InP would be calculated as discussed in Section II-1.

Modified Experimental Procedure

Using the developed theory in Section III-5, a modified experimental procedure was designed to successfully measure the elastic constants of InP. This modified procedure consisted of two processes. The first process was crystal preparation. In addition to the preparations done by INRAD, the InP crystals were first cleaned and glued to the transducers with silver paint. Silver paint was chosen since it provided a good acoustically transparent bond without increasing the impurity level of the InP. As previously explained, X-cut and Y-cut quartz were used as transducers. Second, to insure a good bond, the crystals were baked at 70°C for three hours and allowed to cool to room temp -ature. Third, the transducer leads were soldered to a SMA RF feedthrough. Fourth, the entire subsystem was placed within the environmental chamber. Fifth, the SMA connector was attached to one end of a coaxial cable, passing through the walls of the environmental chamber. Finally, the other end of the cable was connected to the input

terminals of the WK bridge. Thus the crystal preparation process was completed. The next step was to collect data as a function of temperature.

The second process was data collection. Since the modified technique used most of the original technique, as explained in Sections III-2 and III-3, only the changes made or processes not previously explained will be presented. Data collection consisted of several steps. Since preliminary testing indicated that the modified technique could detect resonance, all equipment was first turned on and allowed to warm up and stabilize. Second, the counter was reset, the enable switch turned off, the FM DC input switch of the signal generator was disabled, and an f_{cw} around 10 MHz was selected. An f_{cw} around 10 MHz was chosen since this was the specified resonant frequency of the transducer as given by the manufacturer, Valpey Fisher Corp. Third, the bridge was balanced to closely examine a selected frequency window around 10 MHz. Fourth, the frequency dial of the signal generator was adjusted to coarsely tune f_{cw} to f_o, using the spectrum analyzer and oscilloscope as visual checks. Fifth, the enable switch and the FM DC input switch were turned on, and the FM deviation lowered to the minimum frequency deviation. Finally, readings were taken of the detected f_o from the frequency counter after the measuring system had locked onto f_o, the resonant frequency. The temperature setting of the environmental chamber was varied over 0.0°C to 45.0°C to obtain the temperature dependence of the resonant frequencies. Thus, this second process was repeated for various plates using either longitudinal or shear wave propagation over the 0.0°C to 45.0°C temperature range. These first

two processes are significant for reasons discussed in Section II-2. All the crystal preparations and operation of the system near resonance minimized the possible miscellaneous losses that could have occurred such as acoustic and reflection loss. Minimization of such losses and error resulted in highly confident data values.

These two processes in addition to the original technique made up the modified experimental technique. Data was thus collected accurate to the tens of Hz. The next major task was to arrange the collected data into more meaningful results.

Experimental Results

Presentation of the results of the InP research required several major steps. The first major step was data processing. Having collected the raw frequency data, these values first had to be processed into a more meaningful form. First the raw frequency data was collected. These were the locations of the peaks of the resonant frequencies. From these values a Δf_C was computed for successive peaks. In accordance with the derived theory, this Δf_C was then multiplied by 1.0217 to obtain Δf_{InP}, if a shear wave had been propagated through the crystal. If a longitudinal wave had been propagated through the crystal, Δf_C was multiplied by 1.0301 to obtain Δf_{InP}. Thus:

$$1.0217 = 1 + \frac{M_T}{M_{InP}} \quad \text{(shear wave)} \qquad (3\text{-}29)$$

$$1.0301 = 1 + \frac{M_T}{M_{InP}} \quad \text{(longitudinal wave)} \qquad (3\text{-}30)$$

These values of $(1 + M_T/M_{InP})$ were easily determined since both trans-

ducer and crystal had the same cross-sectional area. Recalling a form of equation 3-11:

$$M = \rho a l \tag{3-31}$$

where M is the mass of the specimen, l is the length, and a is the cross-sectional area. Applying equation 3-31 twice results in:

$$\frac{M_T}{M_{InP}} = \frac{\rho_T l_T a_T}{\rho_{InP} l_{InP} a_{InP}} \tag{3-32}$$

Since $a_T = a_{InP}$, equation 3-32 becomes:

$$\frac{M_T}{M_{InP}} = \frac{\rho_T l_T}{\rho_{InP} l_{InP}} \tag{3-33}$$

But ρ_T is 2649 kg/m^3 [Ref. 20: 48], ρ_{InP} is 4787 kg/m^3 [Ref. 4: 23], l_T (shear wave) is 0.195 millimeters, l_T (longitudinal wave) is 0.270 millimeters, and l_{InP} is 4.970 millimeters. Therefore:

$$1.0217 = 1 + \frac{M_T}{M_{InP}} \quad \text{(shear wave)} \tag{3.29}$$

$$1.0301 = 1 + \frac{M_T}{M_{InP}} \quad \text{(longitudinal wave)} \tag{3-30}$$

Thus applying equations 3-29 and 3-30 to equation 3-28 results in:

$$\Delta f_{InP} = 1.0217\ \Delta f_C \quad \text{(shear wave)} \tag{3-34}$$

$$\Delta f_{InP} = 1.0301\ \Delta f_C \quad \text{(longitudinal wave)} \tag{3-35}$$

After computing Δf_{InP} for a particular temperature an average Δf_{HH} was derived by summing up all the Δf_{InP}'s computed at that temperature (usually 8 to 10 computations), and dividing by the number of computa-

tions. Thus, for a particular plate at a particular temperature, an average Δf_{HH} was computed. These values were tabulated with respect to temperature and are listed as Δf_{HH} in the second columns of Tables D-1, D-2, D-3, D-4, and D-5. These Δf_{HH} values are accurate to the tens of Hz. From these Δf_{HH} values for InP, the corresponding wave velocities were computed applying the theory from Section II-1 and the relation below:

$$v = 2T\ (\Delta f_{HH}) \tag{3-36}$$

where T is 4.970 millimeters, the thickness of the InP samples. Note a factor of 2 shows up since the crystal has only one transducer bonded to it. These wave velocities are listed as velocity in the third columns of Tables D-1, D-2, D-3, D-4, and D-5. Applying equation 3-36 to equation 2-7 results in:

$$c_{eff} = \rho v^2 \tag{3-37}$$

These values are listed as c_{eff} in the fourth columns of Tables D-1, D-2, D-3, D-4, and D-5.

The second step was data analysis. First, the frequency results were tabulated with respect to temperature, the plate orientation, the boule source, and the type of wave propagated. Second, a bivariate linear regression curve using minimum mean square error (MMSE) criteria was then applied to the raw frequency data using temperature as the independent variable, and the change in frequency, Δf_{HH}, as the dependent variable. Third, randomly selected data points from Tables D-1, D-2, D-3, D-4, and D-5, and the resulting "best fit" lines were respectively

plotted in Figures IV-1, IV-2, IV-3, IV-4, and IV-5. Since the temperature range examined was small with respect to the possible temperature range at which an InP device could operate, it was reasonable to assume the data could be approximated by a straight line. It should be noted that the "best fit" curves were calculated to minimize the mean square error of those experimentally determined Δf_{HH} values from a theoretical straight line and not to the room temperature values as previously measured by Hickernell. [Ref. 5: 462] The resulting c_{eff}'s derived from these "best fit" Δf_{HH} values are listed in the fifth columns of Tables D-1, D-2, D-3, D-4, and D-5. These "best fit" c_{eff} values are listed as c'_{eff}, and complete Tables D-1, D-2, D-3, D-4, and D-5.

With these c'_{eff}'s the elastic constants of InP for various selected temperatures were computed. These values are listed in Tables D-6, D-7, and D-8. To derive c_{11}, c_{12}, and c_{44}, three data tables were needed. In the case of generating Table D-6, Tables D-2, D-4, and D-5 were used. In the case of generating Table D-7, Tables D-1, D-4, and D-5 were used. In the case of generating Table D-8, Tables D-2, D-3, and D-4 were used. Thus the elastic constants of InP were derived and from Tables D-6, D-7, and D-8, many relationships can be deduced.

The first major result concerns the temperature dependence of the InP crystals. From Tables D-6, D-7, and D-8, the temperature dependence can be calculated for a specific elastic constant. For the elastic constant c_{11}, the estimated temperature dependence with a 99.0% confidence level is approximately 60 ppm based on the three demonstrated frequency changes over the temperature range for c_{11} found in Tables D-6, D-7, and D-8. Likewise, for the elastic constant c_{12}, the estimated temperature

dependence with a 99.0% confidence level is approximately 70.5 ppm. For the elastic constant c_{44}, the estimated temperature dependence with a 99.9% confidence level is approximately 18 ppm.

The second major result concerns the correlation of the room temperature values of this InP research with those measured by Hickernell in 1965. [Ref. 5: 462] Concerning the elastic constants, Table III-1 compares the values of this InP research with that of the Hickernell study. Concerning the accuracy of the values of the elastic constants of this InP research, all values are accurate to the 4th decimal place or 10^6 N/m^2. Since ρ_{InP} is accurate to 4 significant figures [Ref. 4: 22], T to 4 significant figures, and Δf_{HH} to 5 significant figures, it would appear c_{eff} is accurate to 4 significant figures or 10^7 N/m^2. However, ρ_{InP} (4787 kg/m^3) and T (4.970 mm) do not vary significantly (if at all) over the examined temperature range, and can be considered constants. Thus, the value of c_{eff} strictly depends on Δf_{HH}. Therefore c_{eff} is accurate to the 4th decimal place or 10^6 N/m^2. This accuracy, however, should not be equated with the uncertainty calculations found in Tables III-1 and III-2. Error calculations for these tables are based on the 1965 Hickernell methodology [Ref. 5] and were used to compare the 1965 Hickernell values with those of this research.

TABLE III-1: InP Elastic Constants at Room Temperature.

Elastic Constant	Hickernell	Poe
c_{11}	10.22 ($\pm$ 0.074)	10.2193 ($\pm$ 0.0023)
c_{12}	5.76 ($\pm$ 0.054)	5.7643 ($\pm$ 0.0037)
c_{44}	4.60 ($\pm$ 0.024)	4.6020 ($\pm$ 0.0020)

Note: All elastic constants are measured in 10^{10} N/m^2, and uncer-

tainty factor was calculated using 1965 Hickernell methodology. This methodology expresses the elastic constant as the average experimental value and the uncertainty factor as the spread from the most deviant value to the average. For example in this research c_{11} equals 10.217 (Table D-6), 10.221 (Table D-7), and 10.220 (Table D-8). The average value of these three c_{11}'s is 10.2193. The maximum deviation is 10.2193 - 10.2170 = 0.0023. Thus $\pm$ 0.0023 is the uncertainty factor.

In comparing the two studies, the room temperature elastic constants differ very little from each other. In fact the difference between similar elastic constants lies within the experimental error of either study. For the c_{11} elastic constant the difference is 0.0007, which is well within $\pm$ 0.074 (Hickernell study) or $\pm$ 0.0023 (Poe study). For the c_{12} elastic constant the difference is 0.0043, which is well within $\pm$ 0.054 (Hickernell study) and close to $\pm$ 0.0037 (Poe study). For the c_{44} elastic constant the difference is 0.002, which is well within $\pm$ 0.024 (Hickernell) and $\pm$ 0.0020 (Poe). Thus concerning the elastic constants of InP at room temperature, it is reasonable to assume that the results of this study match those of the 1965 Hickernell study.

Concerning the wave velocities, Table III-2 compares the values of this InP Research with those of the Hickernell study. Concerning the accuracy of the values of the wave velocities of this InP research all values are accurate to 4 significant figures or to the meters per second.

TABLE III-2: InP Wave Velocities at Room Temperature.

Plate Orientation	Mode	Hickernell	Poe
<100>	shear	no value	3.102 ($\pm$0.001)
<110>	shear, type 1	2.160 ($\pm$0.003)	2.157 ($\pm$0.001)
<110>	shear, type 2	3.103 ($\pm$0.004)	3.103 ($\pm$0.001)
<110>	longitudinal	5.130 ($\pm$0.010)	5.131 ($\pm$0.002)
<111>	shear	2.524 ($\pm$0.005)*	2.512 ($\pm$0.001)

Note: all wave velocities are measured in 10^3 m/sec.
*: predicted Hickernell value was 2.510 x 10^3 m/sec.

In comparing the wave velocities of the two studies, the values differ very little from each other. All values derived in this study either exactly match those of the 1965 Hickernell study or are well within the experimental error of the 1965 Hickernell study. For the <111> orientation shear wave case, Hickernell predicted 2.510 km/sec which is well within the experimental error, $\pm$ 0.005, to 2.512 km/sec, the value derived in this study. Thus concerning the wave velocities of InP at room temperature, it is reasonable to assume that the results of this study match those of the 1965 Hickernell study.

The third major result concerns the absolute values of the elastic constants. Based on the three corresponding values of c_{11} listed within Tables D-6, D-7, and D-8, the c_{11} elastic constant at 0.0°C appears to be accurate to the fifth significant digit or 1×10^7 N/m^2. The c_{11} elastic constant at 45.0°C, however, *appears* to be accurate to 8×10^7 N/m^2. Overall, there appears to be a 99.9% confidence level in the absolute values of the c_{11} elastic constant. Likewise, the c_{12} elastic constant at 0.0°C appears to be accurate to the fourth significant digit or 1×10^7 N/m^2. The c_{12} elastic constant at 45.0°C appears to be accurate to 2×10^7 N/m^2. Overall, there appears to be a 99.8% confidence level in the absolute values of the c_{12} elestic constant. The c_{44} elastic constant at 0.0°C appears to be accurate to the fourth significant digit or 1×10^7 N/m^2. The c_{44} elastic constant at 45.0°C appears to be accurate to 3×10^7 N/m^2. Overall, there appears to be a 99.9% confidence level in the absolute values of the c_{44} elastic constant.

Since the c_{44} elastic constant required the least mathematical computations, analysis of c_{44} probably best demonstrates the confidence level

of the data collected. Thus Table D-9 was constructed. Column 2 represents the data collected from Table D-5. Column 3 represents the data collected from Table D-3. Theoretically, since the linear expansion coefficient is negligible over the examined temperature range, Columns 2 and 3 of Table D-9 should differ by approximately 1.1×10^8 N/m^2. This number was derived from the following relation:

$$1.1 \times 10^8 = \frac{e_{14}^2}{\epsilon_{11}} \quad \text{(at room temperature)} \tag{3-36}$$

where e_{14} is the piezoelectric constant and equal to 0.11 C/m^2, and ϵ_{11} is the dielectric constant equal to 1.093×10^{-10} F/m. [Ref. 4: 23] The actual difference between Columns 2 and 3 is listed as e_{14}^2/ϵ_{11} in Column 4 of Table D-9. The room temperature deviation of the measured e_{14}^2/ϵ_{11} is 0.3×10^8 N/m^2. This would also be the maximum deviation of the c_{44} elastic constant at room temperature. The percent error then is simply:

$$0.00065 = \frac{0.3 \times 10^8 \text{ N/m}^2}{4.6 \times 10^{10} \text{ N/m}^2} = 0.065\% \tag{3-37}$$

assuming the Hickernell room temperature value of c_{44} is correct. The confidence level is 1 minus the percent error, and is 99.87% or approximately 99.9%. Thus all the data would appear to be anywhere in the 99.8% to 99.9% confidence level.

For both the relative temperature dependence and absolute values of the elastic constants, the linear coefficient of expansion for InP was not considered. This is because for the observed temperature range, the maximum linear coefficient of expansion is 6.6×10^{-9} m per meter of crystal thickness at 45.0°C. [Ref. 1: 263] Such a value would make

negligible contributions to the change in frequencies with respect to the thickness of the InP crystal. The maximum changes would be in the seventh significant digit of thickness, causing a maximum 0.0000007% change which is at least 10,000 times less than the least significant digit. The average change due to thermal expansion would be far less than 0.0000007%. Thus since thermal expansion would only cause a very insignificant change in the thickness of the crystal, its contribution was ignored. In summarizing the results of this InP research, it appears that the data is of a high confidence level (99.9%), correlates well with itself and the 1965 Hickernell study, and demonstrates low temperature dependence. It should be noted that to obtain such results that samples from both Boule #1 and Boule #2 were used. This would indicate that the precipitation of Fe in the InP did not affect the acoustic wave propagating through the InP.

IV. Conclusions and Recommendations

Experimental System

The elastic constants of InP and temperature coefficients were thus measured over the temperature range from 0.0°C to 45.0°C. The conclusion of this research fall into three major categories. The first category concerns the experimental system used to measure the InP. The second category concerns the results and data that the system produced. The third category concerns the characteristics of the InP used in this research. Concerning the first category, a rather simple and accurate system was designed, constructed, and tested to measure the frequency changes in InP and eventually derive the elastic constants of InP from these measured frequency changes. Although it did not successfully measure the frequency changes of InP without some modifications, the original system did successfully measure the frequency changes of quartz with respect to temperature. This system also has the capabilities to be automated for extensive data collection, and refined for even higher accuracy. Future attention could be put toward increasing the resolution of the system with an automated data acquisition subsystem capable of measuring frequency properties on any piezoelectric material. Such effort could be applied to further studies of InP, which would help InP reach a higher state of maturity.

Summary of Data

The second category concerns the results of this InP research. The first set of conclusions focuses on the wave velocities and elastic con-

stants of InP at room temperature. As previously discussed in Section III-8, the results of this research closely match those derived in the 1965 Hickernell study. The wave velocities of InP from this research are in close agreement with the 1965 Hickernell study. The largest difference is 0.14%, while the average is 0.06%. If all the wave velocities were rounded to the tens of m/sec, all corresponding values of both studies would exactly match. Thus the wave velocities of InP at room temperature are in excellent agreement with the 1965 Hickernell study. In addition, the elastic constants at room temperature are in excellent agreement with those of the 1965 Hickernell study and the 1982 Henaff study. [Ref. 4: 22] Since the elastic constants match so well, it is reasonable to assume that c_{11} equals 10.2193×10^{10} N/m^2 ($\pm$ 0.0023×10^{10} N/m^2), c_{12} equals 5.7643×10^{10} N/m^2 ($\pm$ 0.0037×10^{10} N/m^2), and c_{44} equals 4.6020×10^{10} N/m^2 ($\pm$ 0.0020×10^{10} N/m^2). If the elastic constants were rounded to the nearest 10^8 N/m^2, all elastic constants from all three studies would exactly match. Thus the elastic constants at room temperature from this research are in excellent agreement with the 1965 Hickernell study and the 1982 Henaff study.

The second set of conclusions focuses on the values of the elastic constants of InP as a function of temperature. Although there are no previous studies to compare results with, the final results can be compared with each other. Tables D-6, D-7, and D-8 present the derived elastic constants for various temperatures. Each table represents a different set of three wave propagation cases used to derive the elastic constants. For a particular temperature and elastic constant, all three tables were compared with each other. The deviations between all three

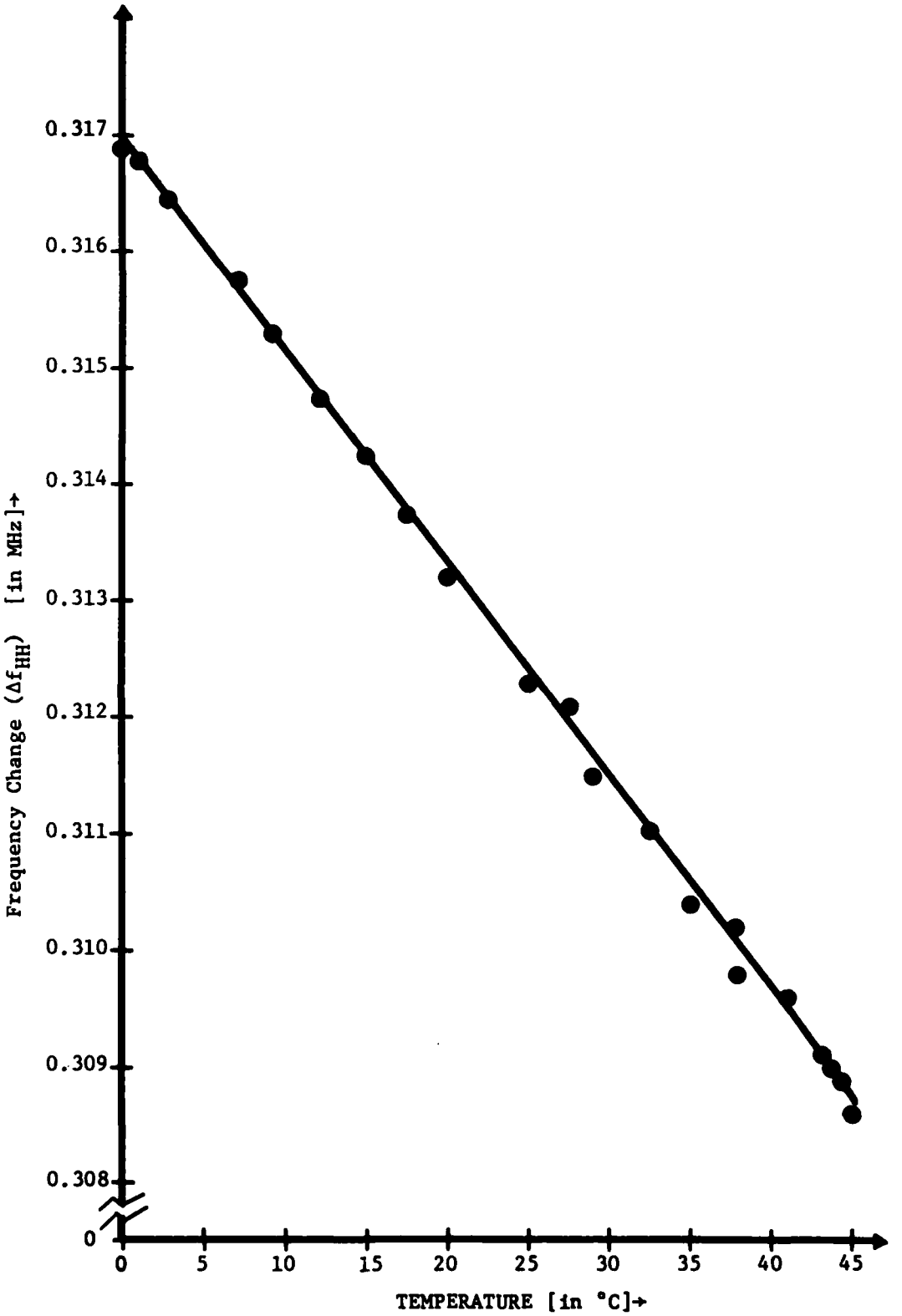

Figure IV-1. Frequency change vs temperature for Thick Plate #11, <111> plane, shear wave propagation.

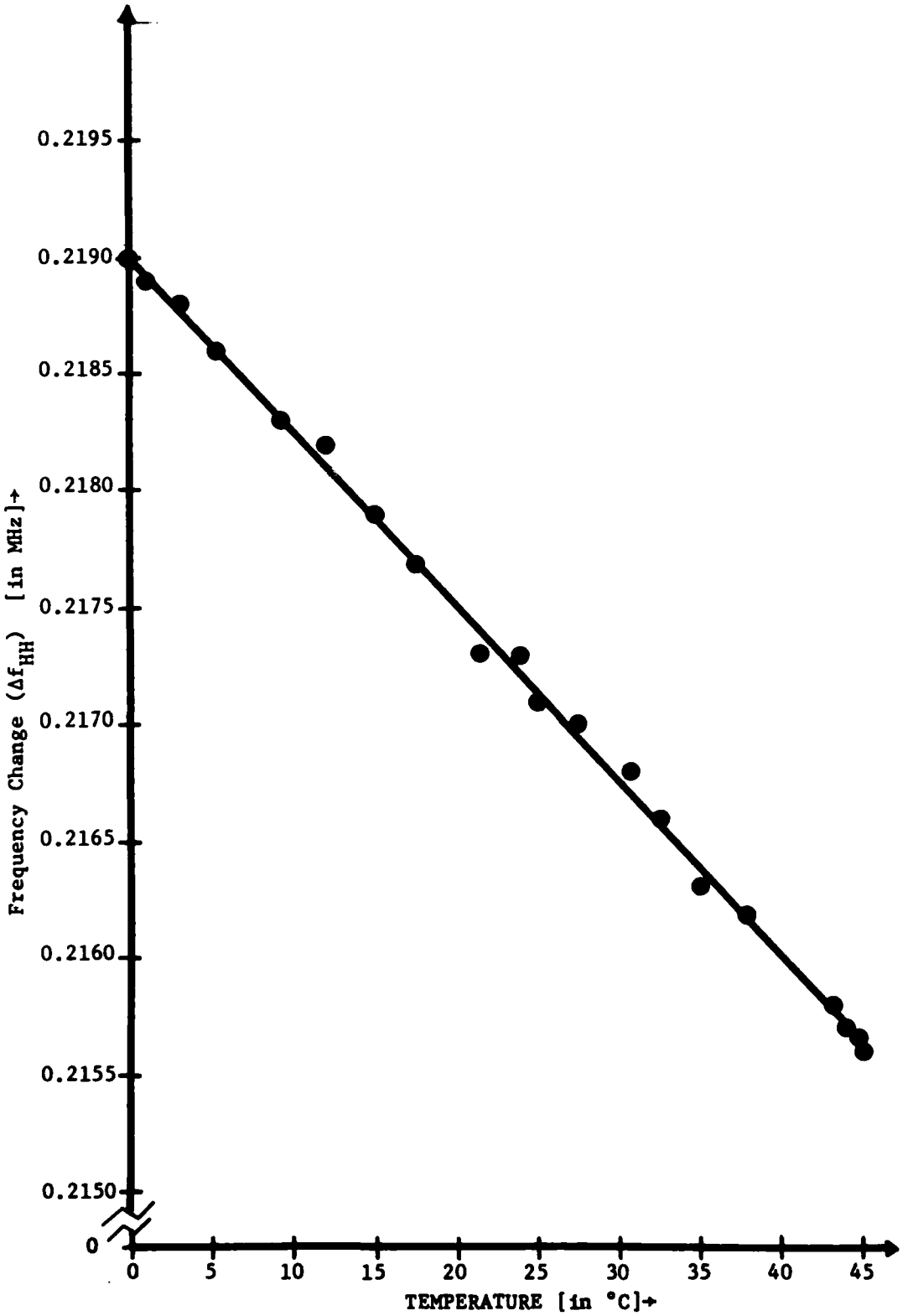

Figure IV-2. Frequency change vs temperature for Thick Plate #22, <110> plane, shear wave propagation, type #1.

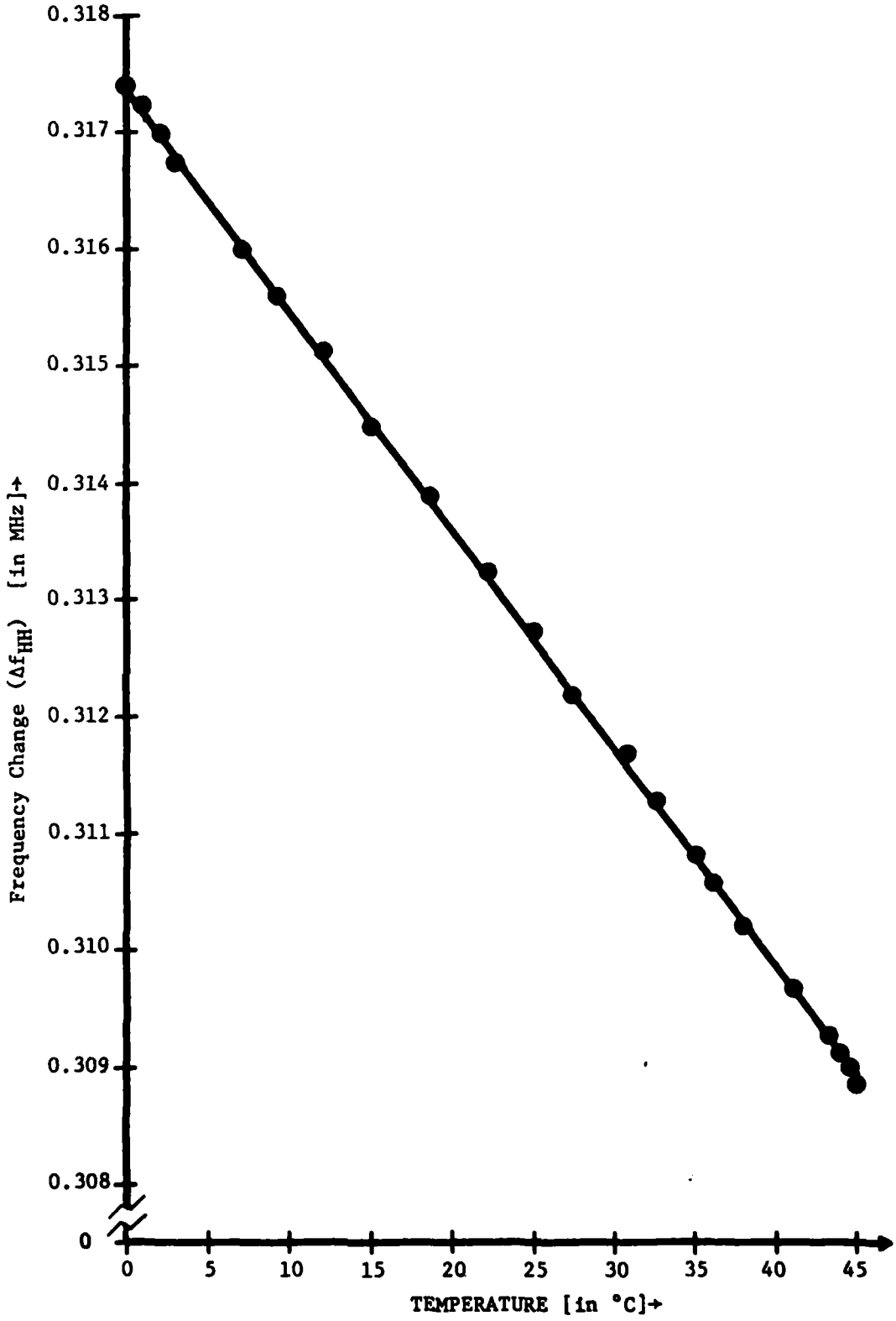

Figure IV-3. Frequency change vs temperature for Thick Plate #22, <110> plane, shear wave propagation, type #2.

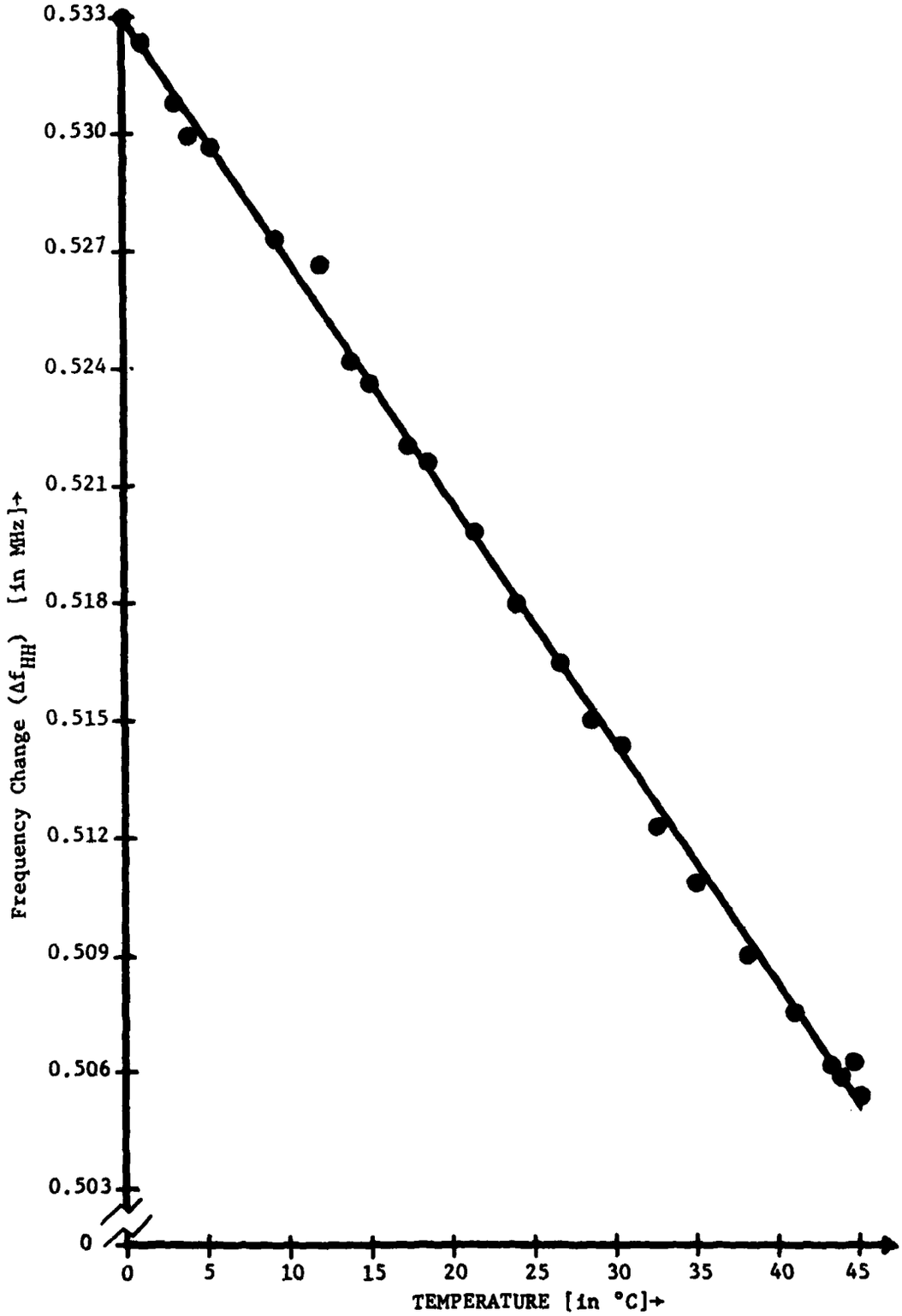

Figure IV-4. Frequency change vs temperature for Thick Plate #22, <110> plane, longitudinal wave propagation.

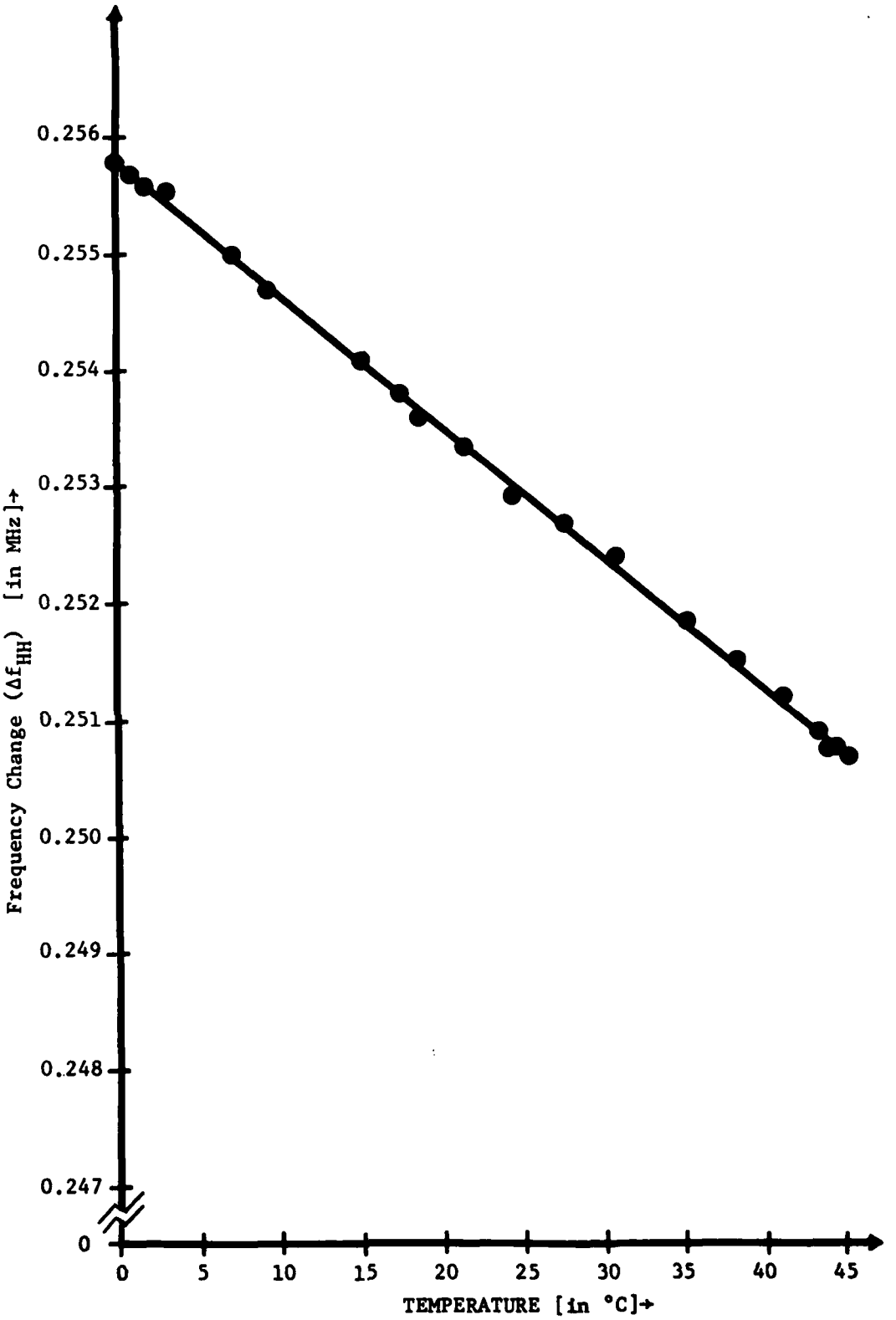

Figure IV-5. Frequency change vs temperature for Thick Plate #32, <100> plane, shear wave propagation.

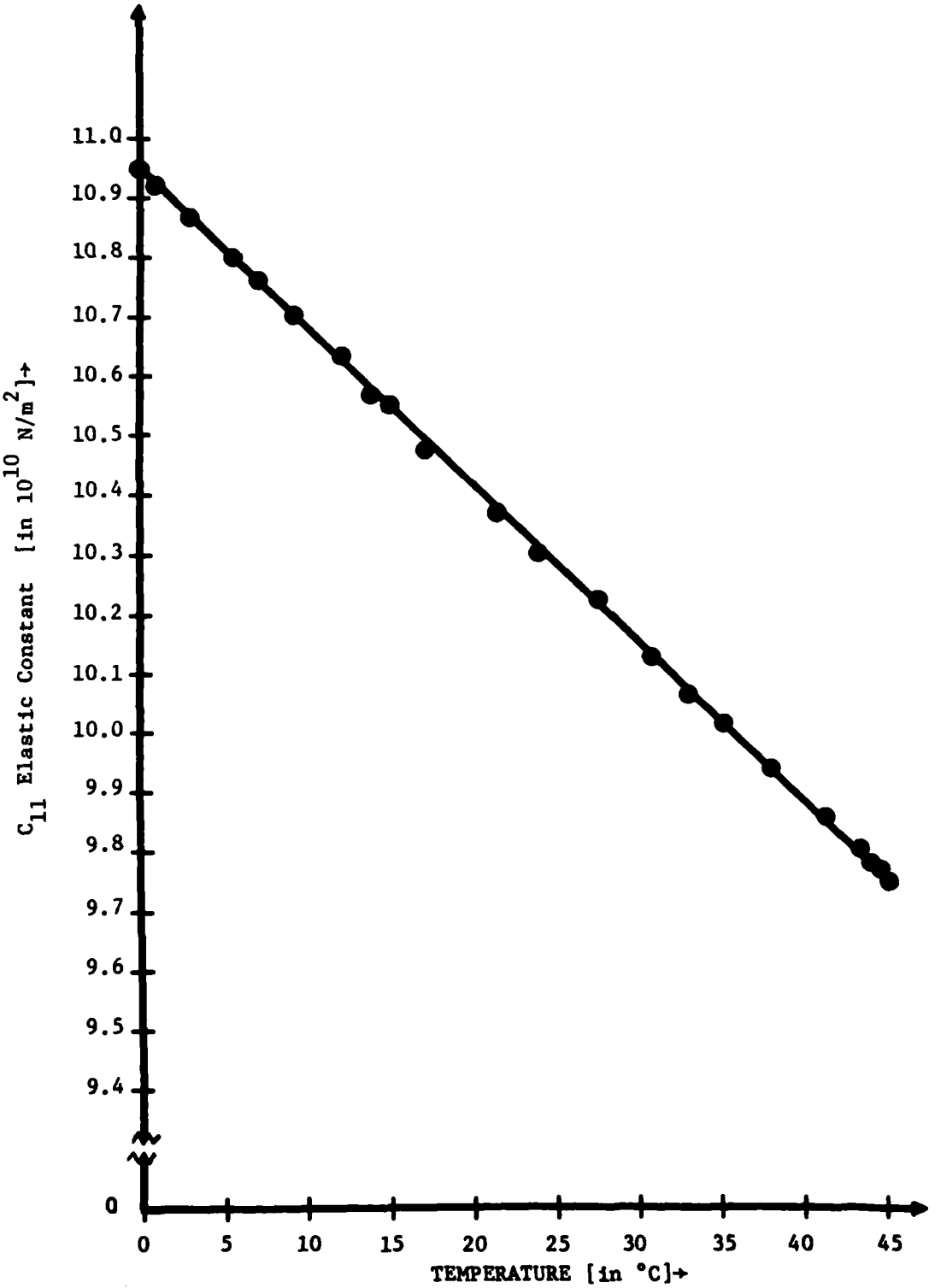

Figure IV-6. C_{11} Elastic Constant vs temperature.

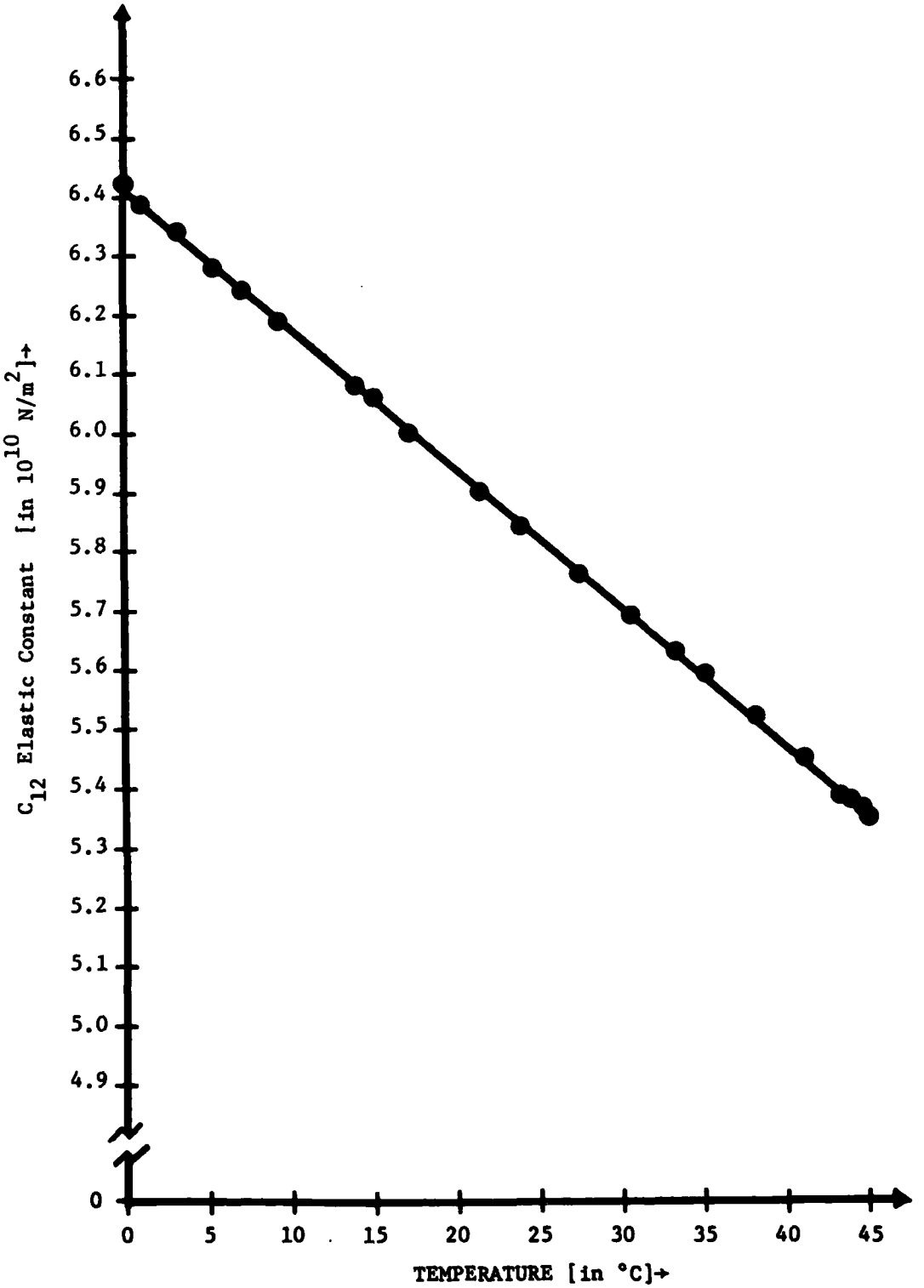

Figure IV-7. C_{12} Elastic Constant vs temperature.

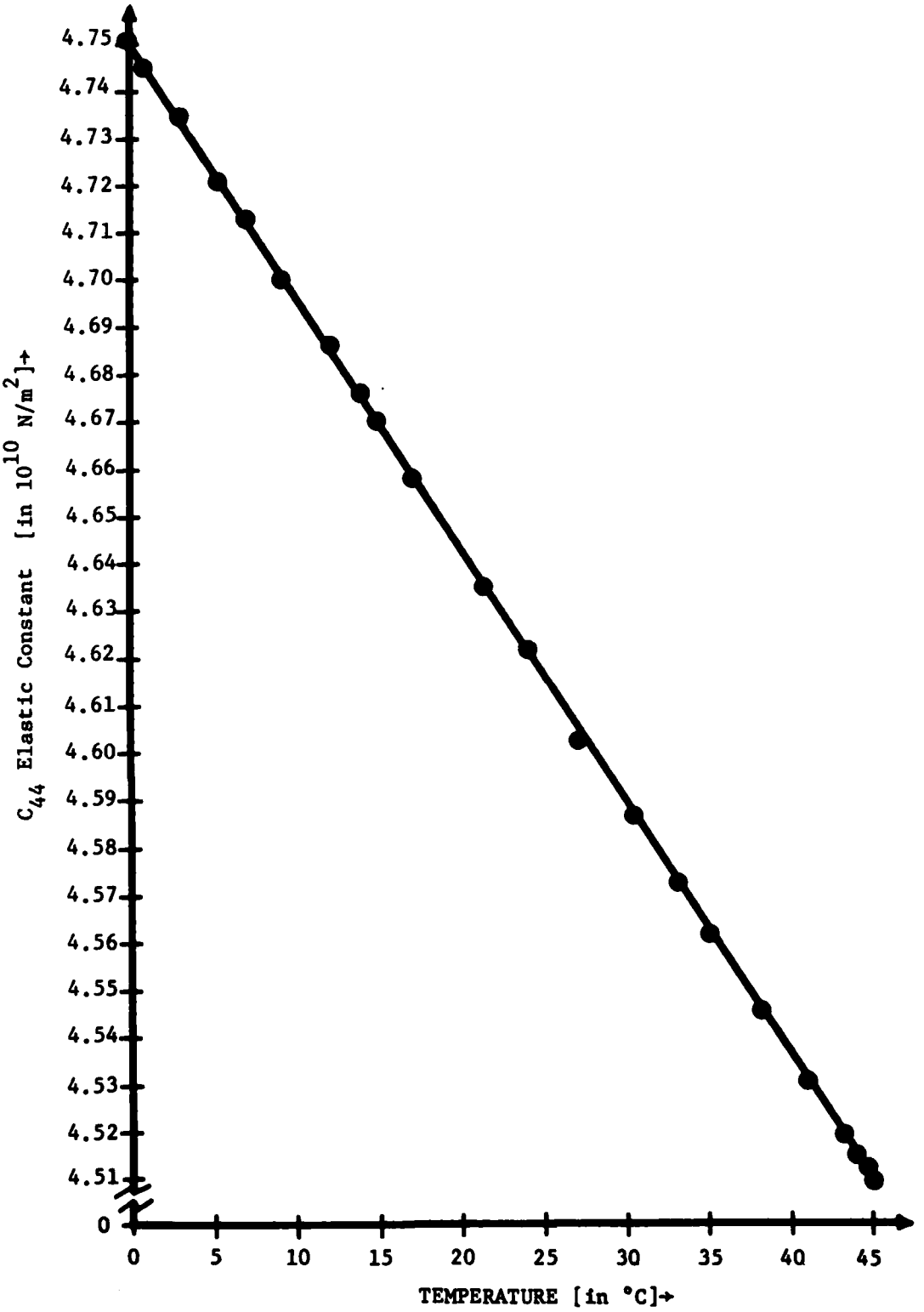

Figure IV-8. C_{44} Elastic Constant vs temperature.

values are so slight that such error calculations suggest a high degree of correlation among the tables, and a high level of confidence in the values themselves. Indeed, the special error calculations presented in Table D-9 and Section III-8 confirm this conclusion. To depict these results graphically, Figures IV-6, IV-7, and IV-8 were drawn. Sample calculations for Figure IV-6 are listed in Table D-10 and D-11. The main source of these calculations was Table D-6. Since all the data on elastic constants, wave velocities, and frequency changes are in excellent agreement with themselves, Figures IV-6, IV-7, and IV-8 are fairly accurate graphs. In addition, since the confidence level is approximately 99.9% for any particular elastic constant at any particular temperature, Figures IV-6, IV-7, and IV-8 summarize in quick visual form the results of this InP research.

The third set of conclusions focuses on the temperature dependence of InP. As seen in Appendix D and Figures IV-1, IV-2, IV-3, IV-4, and IV-5, the frequency change with respect to temperature is small. The changes range from roughly 70 ppm to 18 ppm and decrease with increasing temperature. Such frequency versus temperature curves are similar to frequency versus temperature curves for Indium Antimonide (InSb) [Ref. 9: 37-38] and Gallium Phosphide (GaP) [Ref. 22: 4049]. Low temperature behavior is also exhibited by the wave velocities and elastic constants. The effective elastic constants demonstrate a temperature dependence ranging from 61 ppm to 7 ppm and decrease with increasing temperature. The elastic constants demonstrate a temperature dependence ranging from 71 ppm to 18 ppm and decrease with increasing temperature. Overall, the elastic constants demonstrate small changes as a function of temperature.

With a 99% to 99.9% confidence level in the values of the elastic constants, wave velocities, and changes in the resonant frequencies with respect to temperature, it is reasonable to assume that these derived temperature dependencies are accurate. In short, the temperature dependencies of the elastic constants, wave velocities, and change in the resonant frequencies of InP are quite low. Future attention should be put toward finding directions of propagation for which the temperature coefficient of delay is zero. Such future research would use the data contained in this InP research.

Material Characteristics

The third category concerns the characteristics of the InP. The synthesis process of this research confirmed that the number of impurities, the number of dislocation densities, and the tendency of InP to twin are all inversely related to each other. The crystal preparation process confirmed that InP can be polished and cut to very fine specifications, but there exists a problem in determining if the InP is semi-insulating, especially during boule growth. The experimental procedure produced several conclusions. First, since InP is weakly piezoelectric, piezoelectric excitation may be difficult even with very pure InP. Second, through infrared photography, it was discovered that InP may have regions of precipitated Fe, which will make the InP conductive, and hence not inherently piezoelectrically excitable. Therefore, in addition to publishing the results on the elastic constants of InP, this research has also produced some conclusions on the materials technology of InP.

Overall, this research has confirmed a state of immaturity with InP.

InP, nonetheless, has demonstrated significant potential to the fields of semiconductor and acoustic devices. This research has taken some very important steps in developing the knowledge concerning the material characteristics of InP. From such knowledge InP may soon become a commercially viable product.

Bibliography

1. Bernstein, L. and Beals R. J. "Thermal Expansion and Related Bonding Problems of Some III-V Compound Semiconductors," The Journal of Applied Physics. Vol. 22. pgs. 122-123 (Jan., 1961).

2. Cedrone, N. P. and Curran, D. R. "Electronic Pulse Method for Measuring the Velocity of Sound in Liquids and Solids," The Journal of the Acoustical Society of America. Series 26. pgs. 963-966 (Nov., 1954).

3. Fiarman, R. D. et al. "Recent Progress in the Control of High Purity VPE InP by the PCl_3/InH_2 Technique," Institute of Physics Conference. Series 33. pgs. 45-54 (Jan., 1977).

4. Henaff, J., et al. "Acoustic Wave Propagation on Indium Phosphide Surfaces," Applied Physics Letters. Vol. 41: pgs. 22-24 (July, 1982).

5. Hickernell, F. S. and Gayton, W. R. "Elastic Constants of Single-Crystal Indium Phosphide," The Journal of Applied Physics. Vol. 47. pg. 462 (Jan., 1966).

6. Hilsum, C. and Rees, H. D. "Three-Level Oscillator: A New Form of Transferred Electron Device," Electronics Letters. Vol. 6. pgs. 277-278 (Apr., 1970).

7. Huntington, H. B. "Ultrasonic Measurements on Single Crystals," Physics Review. Vol. 72: pgs. 321-331 (Jan., 1947).

8. Iseler, G. W. Indium Phosphide Materials. ESD TR-80-231. Cambridge, MA: MIT Lexington Lincoln Laboratories, 1980.

9. McSkimin, H. J. "Measurement of Elastic Constants at Low Temperature by Means of Ultrasonic Waves--Data for Silicon and Germanium Single Crystals, and for Fused Silica," Applied Physics. Vol. 24: pgs. 988-997 (Aug., 1953).

10. McSkimin, H. J. "Pulse Superposition Method for Measuring Ultrasonic Wave Velocities in Solids," The Journal of the Acoustical Society of America. Series 33. pgs. 12-16 (Jan., 1961).

11. McSkimin, H. J. "Ultrasonic Methods for Measuring the Mechanical Properties of Liquids and Solids," Physical Acoustics. Vol. I. Part A. Warren P. Mason ed. New York: Academic Press, 1964.

12. McSkimin, H. J. "Use of High Frequency Ultrasound for Determining the Elastic Moduli of Small Specimens," IEEE Transactions on Sonics and Ultrasonics. SU-5: pgs. 25-43 (Aug., 1967).

13. Melcher, R. L., Bolef, D. I., and Merry, J. B. "Frequency Modulation CW Technique for the Measurement of Very Small Changes in Ultrasonic Velocity," The Review of Scientific Instruments. Vol. 39: pgs. 1618-1620 (Nov., 1968).

14. Melcher, R. L., Schickfus, M. V., and Baumann, T. "A New Automatic Method for Measuring Sound Velocity with High Resolution," 1981 Ultrasonics Symposium. pgs. 432-433.

15. Onoe, M., Tiersten, H. F., and Meitzler, A. H. "Shift in the Location of Resonant Frequencies Caused by Large Electromechanical Coupling in Thickness-Mode Resonators," The Journal of the Acoustical Society of America. Vol. 39: pgs. 36-42 (Jan., 1963).

16. Onoe, M., Warner, A. W., and Ballman, A. A. "Elastic and Piezoelectric Characteristics of Bizmuth Germanium Oxide $Bi_{12}GeO_{20}$," IEEE Transactions on Sonics and Ultrasonics. SU-14: pgs. 165-167 (Oct., 1967).

17. Simpson, A. M. et al. "Apparatus for the Continuous Measurement of Changes in Ultrasonic Velocity," The Review of Scientific Instruments. Vol. 51: pgs. 792-794 (June, 1980).

18. Slobodnik, A. J. Jr., and Sethares, J. C. Measurement of the Elastic, Piezoelectric, and Dielectric Constants of $Bi_{12}GeO_{20}$. L. G. Hanscom Field, Bedford, MA: Air Force Cambridge Research Laboratories, 1971. (AFCRL-71-0570).

19. Tiersten, H. F. "Thickness Vibrations of Piezoelectric Plates," The Journal of the Acoustical Society of America. Vol. 35: pgs. 53-58 (Jan., 1963).

20. Tucker, J. W. and Rampton, V. W. Microwave Ultrasonics in Solid State Physics. Amsterdam, The Netherlands: North-Holland Publishing Co., 1972.

21. Vaidyanathan, N. D. et al. Electronic Processes in Indium Phosphide and Related Compounds. Malibu, CA: Hughes Research Laboratories, 1979. (Contract #: N00019-79-C-0082).

22. Weil, R. and Groves, W. O. "The Elastic Constants of Gallium Phosphide," Journal of Applied Physics. Vol. 39: pgs. 4049-4051 (Aug., 1968).

Appendix A

Summary of Elastic Constant Characteristics

TABLE A-1: Elasto-Piezo-Dielectric Matrix for Cubic Crystals in Class 23.

c_{11}	c_{12}	c_{12}	0	0	0	0	0	0
c_{12}	c_{11}	c_{12}	0	0	0	0	0	0
c_{12}	c_{12}	c_{11}	0	0	0	0	0	0
0	0	0	c_{44}	0	0	e_{14}	0	0
0	0	0	0	c_{44}	0	0	e_{14}	0
0	0	0	0	0	c_{44}	0	0	e_{14}
0	0	0	e_{14}	0	0	ε_{11}	0	0
0	0	0	0	e_{14}	0	0	ε_{11}	0
0	0	0	0	0	e_{14}	0	0	ε_{11}

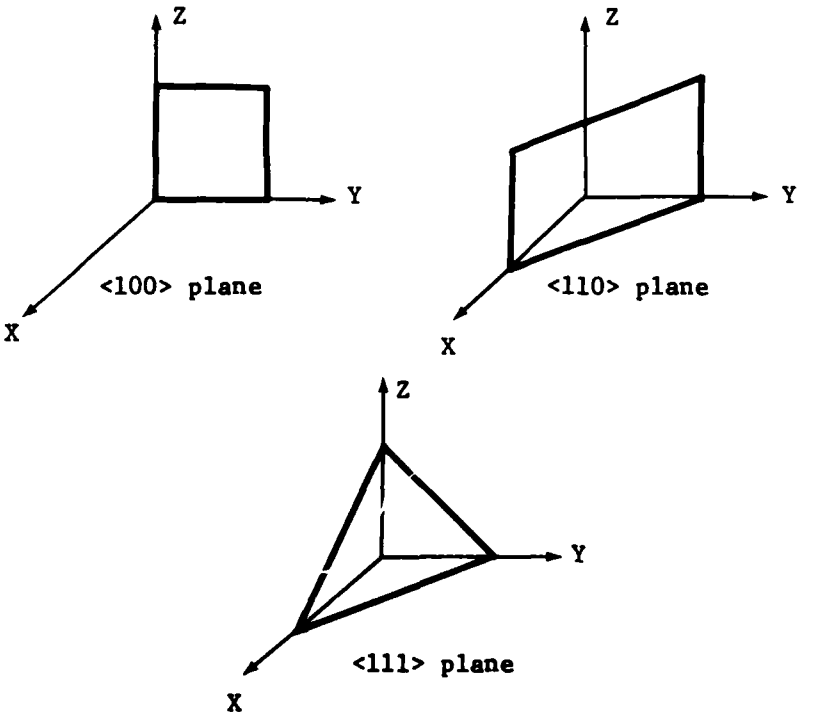

Figure A-1. Plate Orientations which yield pure modes of vibration.

TABLE A-2

Summary of Characteristics for Pure Modes of Vibration for Cubic Crystals of Class 23

Plate Orientation	Mode	Excitation	Direction of Shear Displacement	Effective Elastic Constant c_{eff}	Electromechanical Coupling Factor k
<100>	Extensional	X	---	c_{11}	---
	Shear	$\parallel$	$\perp$ to field	c_{44}	---
<110>	Extensional	$\parallel$ to Z	---	$\frac{c_{11} + c_{12} + 2c_{44}}{2}$	---
	Shear	X	$\perp$ to normal and Z	$\frac{c_{11} - c_{12}}{2}$	---
	Shear	$\perp$	$\parallel$ to Z	$c_{44} + \frac{e_{14}^2}{\varepsilon_{11}}$	$\frac{e_{14}^2}{\varepsilon_{11} c_{eff}}$
<111>	Extensional	$\perp$	---	$\frac{c_{11} + 2c_{12} + 4c_{44}}{3} + \frac{4}{3}\frac{e_{14}^2}{\varepsilon_{11}}$	$\frac{4}{3}\frac{e_{14}^2}{\varepsilon_{11} c_{eff}}$
	Shear	$\parallel$	$\parallel$ to field	$\frac{c_{11} - c_{12} + c_{44}}{3}$	---

$\parallel$ - parallel.

$\perp$ - perpendicular.

X - not piezoelectrically excitable.

AD-A138 454 MEASURING THE TEMPERATURE COEFFICIENTS OF THE ELASTIC CONSTANTS OF INDIUM PHOSPHIDE(U) AIR FORCE INST OF TECH WRIGHT-PATTERSON AFB OH SCHOOL OF ENGI.. J K POE

2/2

UNCLASSIFIED DEC 83 AFIT/GE/EE/83D-59 F/G 9/1 NL

END

DATE FILMED

4-84

DTIC

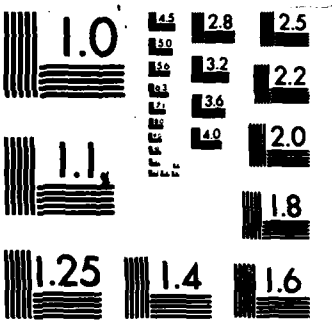

Appendix B

List of Equipment for InP Experimental Measuring System

1. Tektronix Type 555 Dual Beam Oscilloscope
2. Hewlett-Packard 6236B Triple Output Power Supply
3. Princeton-Applied Research Model 184 Lock-In Amplifier
4. Hewlett-Packard 8640B Signal Generator
5. Wayne-Kerr VHF Admittance Bridge
6. Tektronix 7603 Oscilloscope with a 7L12 Spectrum Analyzer Plug In
7. Hewlett-Packard 8447A Amplifier
8. Watkins-Johnson 6201-355 Cascade Amplifier
9. AC/DC Electronics Power Supply
10. Cyborg Thermal P-642 Audio Thermometer
11. Tenney Jr. Environmental Chamber
12. Elite 3 Wiring Board
13. Hewlett-Packard 5340A Electronic Frequency Counter
14. Hewlett-Packard 962B Crystal Detector
15. Indium Phosphide Samples prepared according to specifications (see Appendix C)
16. Miscellaneous Analog Equipment such as resistors, capacitors and operational amplifiers

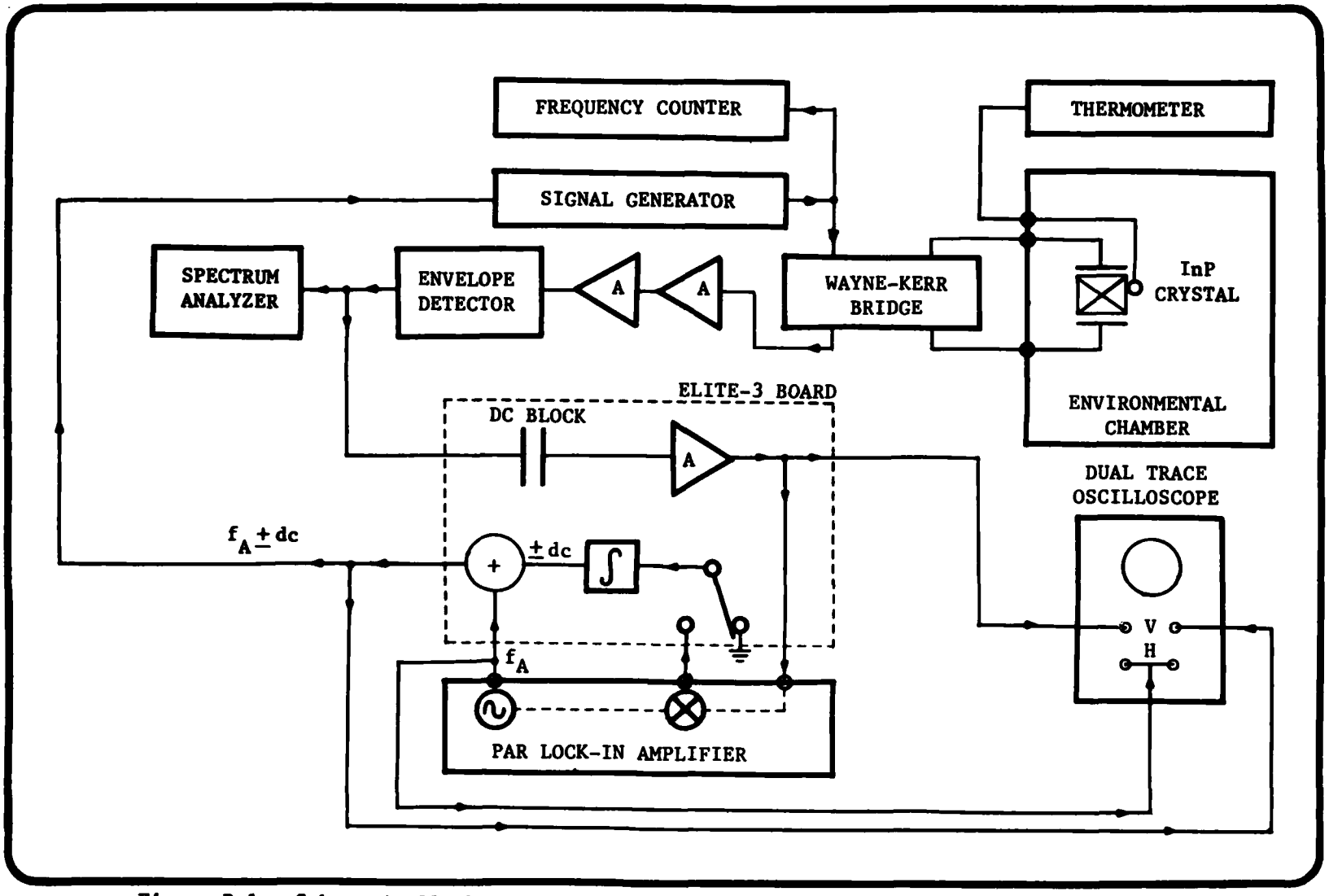

Figure B-1. Schematic Block Diagram of InP Test System to measure resonant frequencies.

Appendix C

Indium Phosphide Crystal Specifications

General Directions:

Use RADC supplied boules. Return any unused material.

Thick Plates:

General Instructions:

1. Size: 11 mm x 10 mm x 5 mm thick.
2. All dimensions to within $\pm$ 0.1 mm, but thickness must be measured to within $\pm$ 0.01 mm and the measured value specified.
3. Both major faces polished flat to within 1/4 wavelength of sodium light or better.
4. Parallelism must be to within 5 seconds of arc or better.
5. All plate orientations must be to within 12 minutes of arc or better.

Detailed Plate Instructions:

1. Thick Plate #1: TP #11:
   a. Quantity = 1, from Boule #1.
   b. Major faces perpendicular to 111 axis.
   c. 10 mm dimension parallel to 110 axis.
   d. Label plate "TP #11".

2. Thick Plate #2: TP #22:
   a. Quantity = 1, from Boule #2.
   b. Major faces perpendicular to 110 axis.
   c. 11 mm dimension parallel to 110 axis.
   d. 10 mm dimension parallel to 001 axis.
   e. Label plate "TP #22".

3. Thick Plate #3: TP #32:
   a. Quantity = 1, from Boule #2.
   b. Major faces perpendicular to 001 axis.
   c. 11 mm dimension parallel to 110 axis.
   d. 10 mm dimension parallel to 110 axis.
   e. Label plate "TP #32".

Small Plates:

General Instructions:

1. Size: 5 mm x 4 mm x 1 mm thick.
2. All dimensions to within ± 0.1 mm, but thickness must be measured to within ± 0.01 mm and the measured value specified.
3. Both faces polished flat to within 1/4 wavelength of sodium light or better.
4. Parallelism must be to within 10 seconds of arc or better.
5. All plate orientations to within 12 minutes of arc or better.

Detailed Plate Instructions:

1. Small Plate #1: SP #1:
   a. Quantity = 2 total, 1 from each boule.
   b. Major faces perpendicular to 111 axis.
   c. 4 mm dimension parallel to 110 axis.
   d. Label "SP #1", and from which boule it came.

2. Small Plate #2: SP #2:
   a. Quantity = 2 total, 1 from each boule.
   b. Major faces perpendicular to 110 axis.
   c. 4 mm dimension parallel to 001 axis.
   d. Label "SP #2", and from which boule it came.

3. Small Plate #3: SP #3:
   a. Quantity = 2 total, 1 from each boule.
   b. Major faces perpendicular to 001 axis.
   c. 4 mm dimension parallel to 100 axis.
   d. Label "SP #3", and from which boule it came.

Irregular Plates:

General Instructions:

1. Size: 11 - 15 mm diameter x 1 mm thick.
2 Diameter must vary between 11 and 15 mm, and must be highly irregular.
3. All dimensions to within ± 0.1 mm, but thickness must be measured to within ± 0.01 mm and the measured value specified.
4. Both faces polished flat to within 1/4 wavelength of sodium light or better (1500 angstroms).
5. Parallelism must be within 10 seconds of arc or better.
6. All plate orientations to within 12 minutes of arc or better.

Detailed Plate Instructions:

1. Irregular Plate #1: IP #11:

   a. Quantity = 1, from Boule #1.
   b. Major faces perpendicular to 111 axis.

2. Irregular Plate #2: IP #21:

   a. Quantity = 1, from Boule #1.
   b. Major faces perpendicular to 110 axis.

Appendix D

Indium Phosphide Data

DATA: TABULAR FORM: TABLE D-1:

Thick Plate #11: <111> Plane: Shear Wave Propagation:

Temperature: in °C	Δf_{HH}: in MHz	Velocity: in m/sec	c_{eff}: in 10^{10} N/m^2	c'_{eff}: in 10^{10} N/m^2
0.00	0.25580	2543	3.095	3.095
1.00	0.25570	2542	3.092	3.092
2.02	0.25560	2541	3.090	3.089
3.01	0.25555	2540	3.089	3.086
5.52	0.25515	2536	3.079	3.080
7.00	0.25500	2535	3.076	3.076
9.40	0.25470	2532	3.068	3.069
10.99	0.25450	2530	3.063	3.065
12.00	0.25445	2529	3.062	3.062
14.00	0.25420	2527	3.056	3.057
15.00	0.25410	2526	3.054	3.054
17.50	0.25380	2523	3.047	3.047
18.49	0.25360	2521	3.042	3.044
21.53	0.25335	2518	3.036	3.036
22.00	0.25330	2518	3.035	3.034
24.00	0.25320	2517	3.032	3.030
25.02	0.25295	2514	3.026	3.027
27.00	0.25275	2512	3.021	3.021
27.37	0.25270	2512	3.020	3.021
28.00	0.25265	2511	3.019	3.019
30.50	0.25240	2509	3.013	3.012
32.52	0.25210	2506	3.006	3.007
33.01	0.25205	2505	3.005	3.005
35.04	0.25185	2503	3.000	3.000
38.01	0.25150	2500	2.992	2.992
41.00	0.25120	2497	2.985	2.984
41.95	0.25115	2496	2.983	2.982
43.25	0.25090	2494	2.977	2.978
44.00	0.25085	2493	2.976	2.976
44.50	0.25075	2492	2.974	2.975
45.00	0.25070	2492	2.973	2.973

Demonstrated frequency change over temperature range = 11.22 ppm.

"Best fit" frequency change over temperature range = 11.32 ppm.

Demonstrated c_{eff} change over temperature range = 0.09% per °C.

DATA: TABULAR FORM: TABLE D-2:

Thick Plate #22: <110> Plane: Shear Wave Propagation: Type #1:

Temperature: in °C	Δf_{HH}: in MHz	Velocity: in m/sec	c_{eff}: in 10^{10} N/m^2	c'_{eff}: in 10^{10} N/m^2
0.00	0.21900	2177	2.268	2.268
1.00	0.21890	2176	2.266	2.267
3.01	0.21880	2175	2.264	2.264
5.52	0.21860	2173	2.260	2.260
7.00	0.21850	2172	2.258	2.258
7.25	0.21830	2170	2.254	2.257
9.40	0.21830	2170	2.254	2.254
11.10	0.21820	2169	2.252	2.251
12.00	0.21820	2169	2.252	2.250
12.11	0.21810	2168	2.250	2.250
13.75	0.21800	2167	2.248	2.247
14.00	0.21795	2166	2.247	2.247
15.00	0.21790	2166	2.246	2.245
17.50	0.21770	2164	2.242	2.241
18.49	0.21760	2163	2.240	2.240
21.53	0.21730	2160	2.233	2.235
24.00	0.21730	2160	2.233	2.231
24.51	0.21720	2159	2.231	2.231
25.02	0.21710	2158	2.229	2.230
27.37	0.21700	2157	2.227	2.226
28.00	0.21690	2156	2.225	2.225
30.50	0.21680	2155	2.223	2.221
31.00	0.21670	2154	2.221	2.221
32.52	0.21660	2153	2.219	2.218
33.01	0.21640	2151	2.215	2.218
35.04	0.21630	2150	2.213	2.214
38.01	0.21620	2149	2.211	2.210
41.00	0.21600	2148	2.209	2.205
41.47	0.21590	2147	2.207	2.205
41.95	0.21585	2146	2.204	2.204
43.25	0.21580	2145	2.203	2.202
44.00	0.21570	2144	2.201	2.201
44.50	0.21565	2144	2.200	2.200
45.00	0.21560	2143	2.199	2.199

Demonstrated frequency change over temperature range = 7.56 ppm.

"Best fit" frequency change over temperature range = 7.46 ppm.

Demonstrated c_{eff} change over temperature range = 0.07% per °C.

DATA: TABULAR FORM: TABLE D-3:

Thick Plate #22: <110> Plane: Shear Wave: Type #2:

Temperature: in °C	Δf_{HH}: in MHz	Velocity: in m/sec	c_{eff}: in 10^{10} N/m^2	c'_{eff}: in 10^{10} N/m^2
0.00	0.31740	3155	4.765	4.764
1.00	0.31725	3153	4.760	4.759
2.00	0.31700	3151	4.753	4.753
3.01	0.31675	3148	4.745	4.747
5.52	0.31630	3144	4.732	4.733
6.02	0.31625	3144	4.730	4.730
7.00	0.31600	3141	4.723	4.725
9.40	0.31560	3137	4.711	4.711
12.00	0.31515	3133	4.698	4.697
14.00	0.31475	3129	4.686	4.686
15.00	0.31450	3126	4.678	4.680
17.50	0.31410	3122	4.666	4.666
18.49	0.31390	3120	4.660	4.661
21.53	0.31340	3115	4.646	4.644
22.00	0.31325	3114	4.641	4.641
24.00	0.31300	3111	4.634	4.630
25.02	0.31275	3109	4.626	4.624
26.01	0.31250	3106	4.619	4.619
27.00	0.31225	3104	4.611	4.614
27.37	0.31220	3103	4.610	4.611
28.00	0.31215	3103	4.609	4.608
30.50	0.31170	3098	4.595	4.594
32.52	0.31130	3094	4.583	4.583
33.01	0.31125	3094	4.582	4.581
35.04	0.31085	3090	4.570	4.569
36.20	0.31060	3087	4.563	4.563
38.01	0.31025	3079	4.553	4.553
41.00	0.30970	3078	4.536	4.536
41.95	0.30950	3076	4.531	4.531
43.25	0.30930	3074	4.525	4.524
44.00	0.30915	3073	4.520	4.520
44.50	0.30900	3071	4.516	4.517
45.00	0.30890	3070	4.513	4.515

Demonstrated frequency change over temperature range = 18.89 ppm.

"Best fit" frequency change over temperature range = 18.68 ppm.

Demonstrated c_{eff} change over temperature range = 0.12% per °C.

DATA: TABULAR FORM: TABLE D-4:

Thick Plate #22: <110> Plane: Longitudinal Wave Propagation:

Temperature: in °C	Δf_{HH}: in MHz	Velocity: in m/sec	c_{eff}: in 10^{10} N/m^2	c'_{eff}: in 10^{10} N/m^2
0.00	0.53290	5297	13.432	13.436
1.00	0.53230	5291	13.401	13.404
2.55	0.53200	5288	13.386	13.356
3.01	0.53075	5276	13.323	13.342
3.90	0.53000	5269	13.286	13.314
5.52	0.52960	5264	13.266	13.264
7.00	0.52875	5256	13.223	13.218
7.75	0.52825	5251	13.198	13.195
9.40	0.52720	5240	13.146	13.144
12.00	0.52690	5237	13.131	13.064
14.00	0.52410	5210	12.992	13.002
15.00	0.52360	5205	12.967	12.971
17.50	0.52200	5188	12.888	12.895
18.49	0.52160	5185	12.868	12.865
21.53	0.51985	5167	12.782	12.771
24.00	0.51800	5149	12.691	12.696
25.02	0.51750	5144	12.667	12.666
25.27	0.51720	5141	12.652	12.658
27.37	0.51615	5131	12.601	12.594
27.80	0.51605	5130	12.596	12.581
28.00	0.51565	5127	12.576	12.575
28.66	0.51505	5119	12.547	12.555
30.01	0.51440	5113	12.515	12.515
30.50	0.51425	5111	12.508	12.500
31.63	0.51310	5100	12.452	12.466
32.52	0.51220	5091	12.408	12.439
33.01	0.51125	5082	12.362	12.424
35.04	0.51085	5078	12.343	12.363
36.85	0.50985	5067	12.295	12.309
37.81	0.51015	5070	12.309	12.280
38.01	0.50900	5058	12.254	12.275
41.00	0.50775	5047	12.194	12.186
41.95	0.50710	5041	12.163	12.157
43.25	0.50615	5032	12.117	12.118
44.00	0.50605	5030	12.112	12.096
44.50	0.50625	5032	12.122	12.082
45.00	0.50525	5022	12.074	12.067

Demonstrated frequency change over temperature range = 61.44 ppm.

"Best fit" frequency change over temperature range = 61.96 ppm.

Demonstrated c_{eff} change over temperature range = 0.24% per °C.

DATA: TABULAR FORM: TABLE D-5:

Thick Plate #32: <100> Plane: Shear Wave Propagation:

Temperature: in °C	Δf_{HH}: in MHz	Velocity: in m/sec	c_{eff}: in 10^{10} N/m^2	c'_{eff}: in 10^{10} N/m^2
0.00	0.31690	3150	4.750	4.751
1.00	0.31680	3149	4.747	4.745
2.33	0.31650	3146	4.738	4.739
3.01	0.31645	3145	4.736	4.735
5.52	0.31600	3141	4.723	4.721
6.71	0.31550	3136	4.708	4.715
7.00	0.31575	3139	4.715	4.713
7.90	0.31580	3139	4.716	4.709
8.01	0.31550	3136	4.708	4.708
9.40	0.31530	3134	4.702	4.700
10.75	0.31490	3130	4.690	4.693
12.00	0.31475	3129	4.686	4.686
14.00	0.31450	3126	4.678	4.676
15.00	0.31425	3124	4.671	4.670
16.02	0.31410	3122	4.666	4.665
17.50	0.31375	3119	4.656	4.656
18.49	0.31350	3116	4.648	4.651
20.00	0.31320	3113	4.640	4.643
21.53	0.31300	3111	4.634	4.635
24.00	0.31238	3105	4.615	4.622
25.02	0.31230	3104	4.613	4.616
27.00	0.31225	3104	4.611	4.605
27.37	0.31210	3102	4.607	4.603
28.00	0.31188	3100	4.601	4.600
29.01	0.31150	3096	4.589	4.595
30.50	0.31130	3094	4.583	4.587
32.52	0.31115	3093	4.579	4.576
33.01	0.31110	3092	4.578	4.573
35.04	0.31040	3085	4.557	4.562
38.01	0.31020	3083	4.551	4.546
38.03	0.30980	3079	4.539	4.546
41.00	0.30960	3077	4.532	4.531
41.95	0.30950	3076	4.531	4.525
43.25	0.30910	3073	4.520	4.519
44.00	0.30900	3071	4.516	4.515
44.50	0.30890	3070	4.513	4.512
45.00	0.30860	3067	4.504	4.509

Demonstrated frequency change over temperature range = 18.44 ppm.

"Best fit" frequency change over temperature range = 18.17 ppm.

Demonstrated c_{eff} change over temperature range = 0.12% per °C.

DATA: TABULAR FORM: TABLE D-6:

ELASTIC CONSTANTS OF INP:

Temperature: in °C	c_{11}: in 10^{10} N/m^2	c_{12}: in 10^{10} N/m^2	c_{44}: in 10^{10} N/m^2
0.00	10.953	6.416	4.751
1.00	10.925	6.391	4.746
3.01	10.871	6.343	4.735
5.52	10.803	6.283	4.721
7.00	10.763	6.247	4.713
9.40	10.698	6.190	4.700
12.00	10.628	6.128	4.686
14.00	10.573	6.079	4.676
15.00	10.546	6.056	4.670
17.50	10.480	5.988	4.656
18.49	10.454	5.974	4.651
21.53	10.371	5.901	4.635
24.00	10.305	5.843	4.622
25.02	10.280	5.820	4.616
27.37	10.217	5.764	4.603
28.00	10.200	5.750	4.600
30.50	10.134	5.692	4.587
32.52	10.081	5.645	4.576
33.01	10.069	5.633	4.573
35.04	10.015	5.587	4.562
38.01	9.939	5.519	4.546
41.00	9.860	5.450	4.531
41.95	9.836	5.428	4.525
43.25	9.801	5.397	4.519
44.00	9.782	5.380	4.515
44.50	9.770	5.370	4.512
45.00	9.749	5.351	4.509

Note: These values of InP were calculated from the following cases:

1. Thick Plate #32: <100> plane: shear wave propagation.
2. Thick Plate #22: <110> plane: shear wave propagation: type #1.
3. Thick Plate #22: <110> plane: longitudinal wave propagation.

Values of the curves derived from this data may be found in Table D-10.

Estimated frequency change over temperature range (based on c'_{eff}):

c_{11} = 60.49 ppm.

c_{12} = 71.01 ppm.

c_{44} = 18.17 ppm.

DATA: TABULAR FORM: TABLE D-7:

ELASTIC CONSTANTS OF INP:

Temperature: in °C	c_{11}: in 10^{10} N/m^2	c_{12}: in 10^{10} N/m^2	c_{44}: in 10^{10} N/m^2
0.00	10.952	6.418	4.751
1.00	10.923	6.393	4.746
3.01	10.869	6.346	4.735
5.52	10.803	6.284	4.721
7.00	10.763	6.248	4.713
9.40	10.698	6.191	4.700
12.00	10.628	6.128	4.686
14.00	10.574	6.079	4.676
15.00	10.547	6.055	4.670
17.50	10.482	5.997	4.656
18.49	10.455	5.974	4.651
21.53	10.373	5.900	4.635
24.00	10.308	5.840	4.622
25.02	10.283	5.818	4.616
27.37	10.221	5.761	4.603
28.00	10.204	5.747	4.600
30.50	10.138	5.689	4.587
32.52	10.086	5.641	4.576
33.01	10.072	5.630	4.573
35.04	10.020	5.582	4.562
38.01	9.944	5.514	4.546
41.00	9.866	5.445	4.531
41.95	9.843	5.422	4.525
43.25	9.807	5.392	4.519
44.00	9.788	5.375	4.515
44.50	9.777	5.364	4.512
45.00	9.763	5.353	4.509

Note: These values of InP were calculated from the following cases:

1. Thick Plate #32: <100> plane: shear wave propagation.
→2. Thick Plate #11: <111> plane: shear wave propagation.
3. Thick Plate #22: <110> plane: longitudinal wave propagation.

Estimated frequency change over temperature range (based on c'_{eff}):

c_{11} = 59.71 ppm.
c_{12} = 71.00 ppm.
c_{44} = 18.17 ppm.

DATA: TABULAR FORM: TABLE D-8:

ELASTIC CONSTANTS OF INP:

Temperature: in °C	c_{11}: in 10^{10} N/m^2	c_{12}: in 10^{10} N/m^2	c_{44}: in 10^{10} N/m^2
0.00	10.951	6.415	4.753
1.00	10.923	6.389	4.748
3.01	10.870	6.342	4.736
5.52	10.802	6.282	4.722
7.00	10.762	6.246	4.714
9.40	10.698	6.190	4.700
12.00	10.628	6.128	4.686
14.00	10.574	6.080	4.675
15.00	10.547	6.057	4.669
17.50	10.471	5.989	4.665
18.49	10.455	5.975	4.650
21.53	10.373	5.903	4.633
24.00	10.308	5.846	4.619
25.02	10.283	5.823	4.613
27.37	10.220	5.768	4.600
28.00	10.203	5.753	4.597
30.50	10.138	5.696	4.583
32.52	10.085	5.649	4.572
33.01	10.072	5.636	4.570
35.04	10.019	5.591	4.558
38.01	9.943	5.523	4.542
41.00	9.866	5.456	4.525
41.95	9.841	5.433	4.520
43.25	9.807	5.403	4.513
44.00	9.788	5.386	4.509
44.50	9.776	5.376	4.506
45.00	9.762	5.364	4.504

Note: These values of InP were calculated from the following cases:

1. Thick Plate #22: <110> plane: shear wave propagation: type #1.
→2. Thick Plate #22: <110> plane: shear wave propagation: type #2.
3. Thick Plate #22: <110> plane: longitudinal wave propagation.

Estimated frequency change over temperature range (based on c'_{eff}):

c_{11} = 59.71 ppm.
c_{12} = 70.04 ppm.
c_{44} = 18.70 ppm.

DATA: TABULAR FORM: TABLE D-9:

C_{44} ELASTIC CONSTANT OF INP:

Temperature: in °C	c_{44}: in 10^{10} N/m^2	$c_{44} + e_{14}^2/\epsilon_{11}$: in 10^{10} N/m^2	e_{14}^2/ϵ_{11}: in 10^8 N/m^2
0.00	4.751	4.764	1.3
1.00	4.745	4.759	1.4
3.01	4.735	4.747	1.2
5.52	4.721	4.733	1.2
7.00	4.713	4.725	1.2
9.40	4.700	4.711	1.1
12.00	4.686	4.697	1.1
14.00	4.676	4.686	1.0
15.00	4.670	4.680	1.0
17.50	4.656	4.666	1.0
18.49	4.651	4.661	1.0
21.53	4.635	4.644	0.9
24.00	4.622	4.630	0.8
25.02	4.616	4.624	0.8
27.00	4.605	4.614	0.9
27.37	4.603	4.611	0.8
28.00	4.600	4.608	0.8
30.50	4.587	4.594	0.7
32.52	4.576	4.583	0.7
33.01	4.573	4.581	0.8
35.04	4.562	4.569	0.7
38.01	4.546	4.553	0.7
41.00	4.531	4.536	0.5
41.95	4.525	4.531	0.6
43.25	4.519	4.524	0.5
44.00	4.515	4.520	0.5
44.50	4.512	4.517	0.5
45.00	4.509	4.515	0.6

Estimated frequency change over temperature range:

c_{44} (column 2) = 18.17 ppm.

c_{44} (column 3) = 18.70 ppm.

Estimated correlation coefficient = 0.999.

Column 2 values from Table D-5.

Column 3 values from Table D-3.

DATA: TABULAR FORM: TABLE D-10:

ELASTIC CONSTANTS OF INP:

LINEAR REGRESSION CURVE FIT CALCULATIONS FOR TABLE D-11:
[using minimum mean square error criteria, (MMSE)]

X variable = temperature in °C
Y variable = elastic constant in N/m^2

c_{11} curve:

Y-intercept	=	10.94767 x 10^{10} N/m^2	(at 0.00°C)
X-intercept	=	9.75126 x 10^{10} N/m^2	(at 45.00°C)
slope	=	-0.026587 x 10^{10} $N/(m^2 \cdot °C)$	
Δ	=	0.0026	= 0.26% per °C
N	=	27.0	
ΣY	=	278.103	
ΣY^2	=	2868.432903	
ΣX	=	657.62	
ΣX^2	=	21592.316	
ΣXY	=	6625.3337	

c_{12} curve:

Y-intercept	=	6.41014 x 10^{10} N/m^2	(at 0.00°C)
X-intercept	=	5.35307 x 10^{10} N/m^2	(at 45.00°C)
slope	=	-0.023490 x 10^{10} $N/(m^2 \cdot °C)$	
Δ	=	0.0041	= 0.41% per °C
N	=	27.0	
ΣY	=	157.626	
ΣY^2	=	923.297242	
ΣX	=	657.62	
ΣX^2	=	21592.316	
ΣXY	=	3708.22408	

c_{44} curve:

Y-intercept	=	4.75071 x 10^{10} N/m^2	(at 0.00°C)
X-intercept	=	4.50894 x 10^{10} N/m^2	(at 45.00°C)
slope	=	-0.0053725 x 10^{10} $N/(m^2 \cdot °C)$	
Δ	=	0.0012	= 0.12% per °C
N	=	27.0	
ΣY	=	124.736	
ΣY^2	=	576.422766	
ΣX	=	657.62	
ΣX^2	=	21592.316	
ΣXY	=	3008.15443	

DATA: TABULAR FORM: TABLE D-11:

ADJUSTED ELASTIC CONSTANTS OF INP
AS DERIVED FROM LINEAR REGRESSION CURVE:

Temperature: in °C	c_{11}: in 10^{10} N/m^2	c_{12}: in 10^{10} N/m^2	c_{44}: in 10^{10} N/m^2
0.00	10.9477	6.4101	4.7507
1.00	10.9211	6.3866	4.7453
5.00	10.8147	6.2927	4.7238
10.00	10.6818	6.1752	4.6970
15.00	10.5489	6.0578	4.6701
20.00	10.4159	5.9403	4.6433
25.00	10.2830	5.8229	4.6164
27.00	10.2298	5.7759	4.6056
27.37	10.2200	5.7672	4.6037
28.00	10.2032	5.7524	4.6003
30.00	10.1501	5.7054	4.5895
35.00	10.0171	5.5880	4.5627
40.00	9.8842	5.4705	4.5358
44.00	9.7778	5.3766	4.5143
45.00	9.7513	5.3531	4.5089

Note: These values were used to draw the curve for their respective figures, Figure IV-6, Figure IV-7, and Figure IV-8. The actual data used to derive these curves is found in Table D-6. Calculations based on that data used to compute the linear regression curves are found in Table D-10. Computer program from Texas Instruments. Calculator used was TI-59.

Estimated frequency change over temperature range:

c_{11} = 60.11 ppm.

c_{12} = 70.49 ppm.

c_{44} = 18.16 ppm.

Appendix E

Analysis of InP Characteristics

Table E-1: Analysis of InP Characteristics

Crystal	Orientation	Surface Resistivity	Bulk Resistivity	IR Photography	Parallelism *	Surface Smoothness
SP#11	<111>	short circuit	---	clear	---	very good
SP#21	<110>	short circuit	13.0Ω	---	0.0115°1 0.0143°w	very good
SP#31	<100>	short circuit	---	cloudy	---	very good
SP#12	<111>	open circuit	$1.5 \times 10^7 \Omega$	---	---	very good
SP#22	<110>	short circuit	---	---	0.0057°1 0.0072°w	very good
SP#32	<100>	open circuit	$1.5 \times 10^7 \Omega$	clear	---	very good
TP#11	<111>	short circuit	---	---	---	very good
TP#22	<110>	open circuit	---	---	---	very good
TP#32	<100>	open circuit	---	---	---	very good
IP#11	<111>	short circuit	2.1Ω	cloudy	0.0191°1 0.0358°w	good
IP#21	<110>	short circuit	---	---	0.0036°1 0.0072°w	good
SP#13a	<111>	open circuit	$2.0 \times 10^7 \Omega$	clear	0.43°1 0.36°w	fair
SP#13b	<111>	open circuit	---	clear	0.44°1 0.34°w	fair
SP#13c	<111>	open circuit	---	---	0.49°1 0.40°w	fair
SP#13d	<111>	open circuit	$1.0 \times 10^7 \Omega$	---	0.37°1 0.33°w	fair
SP#13e	<111>	open circuit	$1.0 \times 10^7 \Omega$	---	0.19°1 0.34°w	fair
SP#33	<100>	open circuit	---	clear	0.37°1 0.34°w	fair

* Note: 1 = longitude, w = latitude

VITA

Jonathan K. W. L. Poe was born 11 March 1960 in Honolulu, Hawaii. He graduated from Iolani High School in Honolulu in 1978. He then attended Cornell University in Ithaca, New York as a Cornell National Scholar on an ROTC scholarship. He received a Bachelor of Science degree in Electrical Engineering from Cornell's College of Engineering in May of 1982. Through the AFROTC program, he received a regular commission in the USAF upon graduation with distinction. Promptly thereafter he entered the Master's of Science Program of the School of Engineering, Air Force Institute of Technology, as his first assignment in June of 1982.

Permanent address: 5410 Oio Drive

Honolulu, Hawaii 96821

UNCLASSIFIED

SECURITY CLASSIFICATION OF THIS PAGE

REPORT DOCUMENTATION PAGE

1a. REPORT SECURITY CLASSIFICATION: UNCLASSIFIED	1b. RESTRICTIVE MARKINGS
2a. SECURITY CLASSIFICATION AUTHORITY	3. DISTRIBUTION/AVAILABILITY OF REPORT: Approved for public release; distribution unlimited
2b. DECLASSIFICATION/DOWNGRADING SCHEDULE	
4. PERFORMING ORGANIZATION REPORT NUMBER(S): AFIT/GE/EE/83D-59	5. MONITORING ORGANIZATION REPORT NUMBER(S)
6a. NAME OF PERFORMING ORGANIZATION: School of Engineering; 6b. OFFICE SYMBOL (If applicable): AFIT/ENG	7a. NAME OF MONITORING ORGANIZATION
6c. ADDRESS (City, State and ZIP Code): Air Force Institute of Technology, Wright-Patterson AFB, OH 45433	7b. ADDRESS (City, State and ZIP Code)
8a. NAME OF FUNDING/SPONSORING ORGANIZATION: Rome Air Development Ctr.; 8b. OFFICE SYMBOL (If applicable): EEA	9. PROCUREMENT INSTRUMENT IDENTIFICATION NUMBER
8c. ADDRESS (City, State and ZIP Code): Rome Air Development Center/EEA, Hanscom AFB, MA 01731	10. SOURCE OF FUNDING NOS. — PROGRAM ELEMENT NO. / PROJECT NO. / TASK NO. / WORK UNIT NO.
11. TITLE (Include Security Classification): see Box 19	

12. PERSONAL AUTHOR(S): Jonathan K. Poe, B.S.E.E., 2d Lt., USAF

13a. TYPE OF REPORT	13b. TIME COVERED	14. DATE OF REPORT (Yr., Mo., Day)	15. PAGE COUNT
MS Thesis	FROM _____ TO _____	1983 December	114

16. SUPPLEMENTARY NOTATION

Approved for public release: IAW AFR 190-17

LYNN E. WOLAVER
Dean for Research and Professional Development
Air Force Institute of Technology (AIC)
Wright-Patterson AFB OH 45433

17. COSATI CODES		
FIELD	GROUP	SUB. GR.

18. SUBJECT TERMS (Continue on reverse if necessary and identify by block number)
Microwave Theory and Techniques; Elastic Constants; Acoustic Waves; Temperature Coefficients; Indium Phosphide; III-V Semiconductor Compounds

19. ABSTRACT (Continue on reverse if necessary and identify by block number)

TITLE: MEASURING THE TEMPERATURE COEFFICIENTS OF THE ELASTIC CONSTANTS OF INDIUM PHOSPHIDE (unclassified)

ABSTRACT:

The temperature dependence of the elastic constants of Indium Phosphide (InP) was measured over the 0.0 °C to 45.0 °C temperature range. A modified Continuous Wave Resonance Technique was used to experimentally determine the values. The calculated temperature dependence was 60 ppm for the c_{11} elastic constant, 70.5 ppm for the c_{12} elastic constant, and 18 ppm for the c_{44} elastic constant. All are negative with increasing temperature. Such behavior is consistent with similiar studies of Indium Antimony (InSb), Gallium Phosphide (GaP), and Gallium Arsenide (GaAs).

The InP technique in this research applies the vibrational theory of small plates developed in 1969 by Tiersten in order to detect acoustic resonances in single crystal

20. DISTRIBUTION/AVAILABILITY OF ABSTRACT	21. ABSTRACT SECURITY CLASSIFICATION
UNCLASSIFIED/UNLIMITED ☒ SAME AS RPT. ☐ DTIC USERS ☐	UNCLASSIFIED

22a. NAME OF RESPONSIBLE INDIVIDUAL	22b. TELEPHONE NUMBER (Include Area Code)	22c. OFFICE SYMBOL
Roger D. Colvin, Capt., USAF	(513) 255-3576	AFIT/ENG

DD FORM 1473, 83 APR — EDITION OF 1 JAN 73 IS OBSOLETE.

UNCLASSIFIED

SECURITY CLASSIFICATION OF THIS PAGE

InP. The change in the resonant frequencies allows calculation of the acoustic wave velocity and corresponding effective elastic constant. By measuring the effective elastic constant for various plate orientations, the elastic constants of InP can be derived. Since InP is a cubic crystal of class 23 with a zinc-blende structure, measurements of the <111>, <110>, and <100> planes are sufficient to compute the elastic constants at a particular temperature. From such computations, changes in the elastic constants can be calculated with respect to temperature. Thus the temperature dependencies for the elastic constants of InP are derived.

The circuitry incorporating this InP technique utilizes a spectrum analyzer, an FM DC coupled signal generator, a high precision frequency counter, and a Wayne-Kerr Bridge. In addition, an analog feedback loop was constructed to allow precision within 1 ppm. Such circuitry could easily be modified for automated data processing and higher precision. This technique and resulting circuitry could be applicable to measuring acoustic properties on any piezoelectrically excitable material as demonstrated by its success on X-cut quartz and InP in this research.


D
FI